On the Nature of the Ultrarelativistic Prompt Emission Phase of GRB 190114C and GRB 180720B

Remo Ruffini,

Y. Aimuratov, L. Becerra, C.L. Bianco, S. Campion, Y.-C. Chen, C. Cherubini, S. Filippi, M. Karlica, L. Li, G.J. Mathews, R. Moradi, M. Muccino, G.B. Pisani, J.A. Rueda, N. Sahakyan, Y. Wang, S.-S. Xue

ICRANet-Isfahan Astronomy meeting – IUT and online, November 3, 2021

Pulsars and Neutron stars rotational energy

$$\left(\frac{dE}{dt}\right)_{obs} \simeq 4\pi^2 \frac{I_{NS}}{P^3}\frac{dP}{dt}$$

Chinese, Japanese, Korean astronomers (1054 A.D.)

R. Oppenheimer & R. Volkoff (1939)

J. Bell & T. Hewish (1967)

UHECRs (2000-2011)

AGILE Flare (2011)

Open issue: the emission of the remnant.

Roy P. Kerr, 1963

GRAVITATIONAL FIELD OF A SPINNING MASS AS AN EXAMPLE OF ALGEBRAICALLY SPECIAL METRICS

Roy P. Kerr*

University of Texas, Austin, Texas and Aerospace Research Laboratories, Wright-Patterson Air Force Base, Ohio

Goldberg and Sachs[1] have proved that the algebraically special solutions of Einstein's empty-space field equations are characterized by the existence of a geodesic and shear-free ray congruence, k_μ. Among these spaces are the plane-fronted waves and the Robinson-Trautman metrics[2] for which the congruence has nonvanishing divergence, but is hypersurface orthogonal.

In this note we shall present the class of solutions for which the congruence is diverging, and is not necessarily hypersurface orthogonal. The only previously known example of the general case is the Newman, Unti, and Tamburino metrics,[3] which is of Petrov Type D, and possesses a four-dimensional group of isometries.

If we introduce a complex null tetrad ($t*$ is the complex conjugate of t), with

$$ds^2 = 2tt* + 2mk,$$

where ζ is a complex coordinate, a dot denotes differentiation with respect to u, and the operator D is defined by

$$D = \partial/\partial\zeta - \Omega\partial/\partial u.$$

P is real, whereas Ω and m (which is defined to be $m_1 + im_2$) are complex. They are all independent of the coordinate r. Δ is defined by

$$\Delta = \mathrm{Im}(P^{-2}D*\Omega).$$

There are two natural choices that can be made for the coordinate system. Either (A) P can be chosen to be unity, in which case Ω is complex, or (B) Ω can be taken pure imaginary, with P different from unity. In case (A), the field equations are

$$(m - D*D*D\Omega) = |\partial_u D\Omega|^2, \tag{2}$$

1. Carry out the separation of variables in the Hamilton–Jacobi equation for a particle moving in the Kerr field (B. Carter, 1968).

Solution: In the Hamilton–Jacobi equation

$$g^{ik} \frac{\partial S}{\partial x^i} \frac{\partial S}{\partial x^k} m^2 = 0$$

(m is the mass of the particle, not to be confused with the mass of the central body) with g^{ik} from (104.6) the time t and the angle ϕ are cyclic variables; they therefore enter in the action S in the form $-\mathscr{E}_0 t + L\phi$, where $\mathscr{E}_0$ is the conserved energy and L denotes the component of the angular momentum along the axis of symmetry of the field. It turns out that the variables θ and r can also be separated. Writing S in the form

$$S = -\mathscr{E}_0 t + L\phi + S_r(r) + S_\theta(\theta), \tag{1}$$

we reduce the Hamilton–Jacobi equation to two ordinary differential equations (cf. *Mechanics*, § 48):

$$\left(\frac{dS_\theta}{d\theta}\right)^2 + \left(a\mathscr{E}_0 \sin\theta - \frac{L}{\sin\theta}\right)^2 + a^2 m^2 \cos^2\theta = K,$$

$$\left(\frac{dS_r}{dr}\right)^2 - \frac{1}{\Delta}[(r^2 + a^2)\mathscr{E}_0 - aL]^2 + m^2 r^2 = -K, \tag{2}$$

where K (the separation parameter) is a new arbitrary constant. The functions S_θ and S_r are then determined by simple quadratures.

The four-momentum of the particle is

$$p^i = m \frac{dx^i}{ds} = g^{ik} p_k = -g^{ik} \frac{\partial S}{\partial x^k}.$$

Calculating the right-hand side of this equation using (1) and (2), we get the following equations:

$$m \frac{dt}{ds} = -\frac{r_g r a}{\varrho^2 \Delta} L + \frac{\mathscr{E}_0}{\Delta}\left(r^2 + a^2 + \frac{r_g r a^2}{\varrho^2} \sin^2\theta\right), \tag{3}$$

$$m \frac{d\phi}{ds} = \frac{L}{\Delta \sin^2\theta}\left(1 - \frac{r_g r}{\varrho^2}\right) + \frac{r_g r a}{\varrho^2 \Delta}\mathscr{E}_0, \tag{4}$$

$$m^2 \left(\frac{dr}{ds}\right)^2 = \frac{1}{\varrho^4}[(r^2 + a^2)\mathscr{E}_0 - aL]^2 - \frac{\Delta}{\varrho^4}(K + m^2 r^2), \tag{5}$$

$$m^2 \left(\frac{d\theta}{ds}\right)^2 = \frac{1}{\varrho^4}(K - a^2 m^2 \cos^2\theta) - \frac{1}{\varrho^4}\left(a\mathscr{E}_0 \sin\theta - \frac{L}{\sin\theta}\right)^2 \tag{6}$$

These integrals are the first integrals of the equations of motion (the equations of the geodesics). The equation of the trajectory and the time dependence of the coordinates along the trajectory can be found either from (3) to (6) or directly from the equations

$$\partial S/\partial\mathscr{E}_0 = \text{const}, \quad \partial S/\partial L = \text{const}, \quad \partial S/\partial K = \text{const}.$$

For the case of light rays, we must set $m = 0$ on the right sides of equations (3)–(6) and write ω_0 in place of $\mathscr{E}_0$ (cf. § 101), while we must replace the derivatives md/ds on the left sides by the derivatives $d/d\lambda$ with respect to the parameter λ, which varies along the ray (cf. the end of § 87).

Equations (4)–(6) permit purely radial motion only along the axis of rotation of the body, as is already clear from symmetry arguments. From these same considerations it is clear that motion in a "plane" is possible only if the plane is equatorial. In that case, setting $\theta = \pi/2$ and expressing K in terms of $\mathscr{E}_0$ and L from the condition $d\theta/ds = 0$, we obtain the equations of motion in the form

$$m \frac{dt}{ds} = -\frac{r_g a}{r\Delta} L + \frac{\mathscr{E}_0}{\Delta}\left(r^2 + a^2 + \frac{r_g a^2}{r}\right), \tag{7}$$

$$m \frac{d\phi}{ds} = \frac{M}{\Delta}\left(1 - \frac{r_g}{r}\right) + \frac{r_g a}{r\Delta}\mathscr{E}_0, \tag{8}$$

$$m^2 \left(\frac{dr}{ds}\right)^2 = \frac{1}{r^4}[(r^2 + a^2)\mathscr{E}_0 - aL]^2 - \frac{\Delta}{r^4}[(a\mathscr{E}_0 - L)^2 + m^2 r^2], \tag{9}$$

2. Determine the radius of the circle, closest to the centre, that is a stable orbit for a particle moving in the equatorial plane of the limiting ($a \to r_g/2$) Kerr field (R. Ruffini and J. A. Wheeler, 1969).

Solution: Proceeding as in problem 1 of § 102, we introduce the "effective potential energy" $U(r)$ defined from

$$[(r^2 + a^2)U(r) - aL]^2 - \Delta[(aU(r) - L)^2 + r^2 m^2] = 0$$

[for $\mathscr{E}_0 = U$ the right side of eq. (9) vanishes]. The radii of stable orbits are determined by the minima of the function $U(r)$, i.e. by simultaneous solution of the equations $U(r) = \mathscr{E}_0$, $U'(r) = 0$ for $U''(r) > 0$. The orbit closest to the centre corresponds to $U''(r_{\min}) = 0$; for $r < r_{\min}$, the function $U(r)$ has no minima. As a result we obtain the following values for the parameters of the motion:

(a) When $L < 0$ (motion opposite to the direction of rotation of the collapsar)

$$\frac{r_{\min}}{r_g} = \frac{9}{2}, \quad \frac{\mathscr{E}_0}{m} = \frac{5}{3\sqrt{3}}, \quad \frac{L}{mr_g} = -\frac{11}{3\sqrt{3}}.$$

(b) For $L > 0$ (motion in the direction of rotation of the collapsar) as $a \to r_g/2$ the radius $r_{\min}$ tends toward the radius of the horizon. Setting $a = (r_g/2)(1 + \delta)$, we find, for $\delta \to 0$:

$$\frac{r_{\text{hor}}}{r_g} = \frac{1}{2}(1 + \sqrt{2\delta}), \quad \frac{r_{\min}}{r_g} = \frac{1}{2}[1 + (4\delta)^{\frac{1}{3}}]$$

Then

$$\frac{\mathscr{E}_0}{m} = \frac{L}{mr_g} = \frac{1}{\sqrt{3}}[1 + (4\delta)^{\frac{1}{3}}].$$

We call attention to the fact that $r_{\min} r_{\text{hor}}$ remains greater than 1 throughout, i.e. the orbit does not go outside the horizon. This is as it should be: the horizon is a null hypersurface, and no timelike world lines of moving particles can lie on it.

Christodoulou, 1970

[10]S. Weinberg, in *Proceedings of the Fourteenth International Conference on High Energy Physics, Vienna, Austria, 1968*, edited by J. Prentki and J. Steinberger (CERN Scientific Information Service, Geneva, Switzerland, 1968).

[11]N. Cabibbo, Phys. Lett. **12**, 137 (1964).

[12]M. Gell-Mann, Phys. Rev. **125**, 1067 (1962), and Physics (Long Island City, N. Y.) **1**, 63 (1964).

[13]M. Gell-Mann, J. Oakes, and B. Renner, Phys. Rev. **175**, 2195 (1968).

[14]S. Okubo, Nuovo Cimento **54A**, 491 (1968), and **57A**, 794 (1968), and Ann. Phys. (New York) **49**, 219 (1968); R. E. Marshak *et al.*, Nucl. Phys. **B11**, 253 (1969).

Reversible and Irreversible Transformations in Black-Hole Physics*

Demetrios Christodoulou

Joseph Henry Laboratories, Princeton University, Princeton, New Jersey 08540
(Received 17 September 1970)

The concepts of irreducible mass and of reversible and irreversible transformations in black holes are introduced, leading to the formula $E^2 = m_{ir}^2 + (L^2/4m_{ir}^2) + p^2$ for a black hole of linear momentum p and angular momentum L.

This note reports five conclusions: (1) The mass energy of a black hole of angular momentum L can be expressed in the form

$$m^2 = m_{ir}^2 + L^2/4m_{ir}^2, \qquad (1)$$

where m_{ir} is the irreducible mass [geometrical units: $L(\text{cm}) = (G/c^3) L_{conv}(\text{g cm}^2/\text{sec})$; $m(\text{cm}) = (G/c^2) M_{conv}(\text{g})$; $G/c^2 = 0.742 \times 10^{-28}$ cm/g] of the black hole. (2) Insofar as one looks apart from the atomicity of matter one can approach arbitrarily closely to reversible transformations that augment or deplete the rotational contribution to the square of the mass. (3) The attainable range of reversible transformation extends[1,2] from $L = 0$, $m^2 = m_{ir}^2$ to $L = m^2$, $m^2 = 2m_{ir}^2$. (Contrast to the formula for mass energy as it depends upon translation, $E^2 = m^2 + p^2$, where p is unlimited; and with the formula for the squared mass energy of a meson!) (4) An irreversible transformation is characterized (Fig. 1) by an increase in the irreducible mass of the black hole. (5) There exists no process which will decrease the irreducible mass.

Roger Penrose has pointed out[3] a way to extract energy from a black hole endowed with angular momentum. It makes use of the "ergosphere" (Ruffini and Wheeler; cf. Fig. 2, reproduced from their paper[4]), the region between the horizon (surface of black hole; boundary of region from which no particle or radiation can ever escape) and the surface of infinite red shift (coincident with the horizon only for case of the angular-momentum–free Schwarzschild black hole). A particle of energy E_0 is sent from infinity into

the ergosphere and decays there into (1) a particle which emerges to infinity with a rest-plus-kinetic energy E_2 greater than E_0, together with (2) a particle ("rocket ejecta") which has an energy E_1, that is negative as measured at infinity ($E_1 = E_0 - E_2$), but positive in the local Lorentz frame, and which is ejected into such a direction that it is captured into the black hole, thereby diminishing its mass. We consider the case where all masses can be regarded as infinitesimal compared with the mass of a black hole.

The energy E, as measured at infinity, of a particle of angular momentum p_φ and rest mass μ, having a turning point at r, is given by the
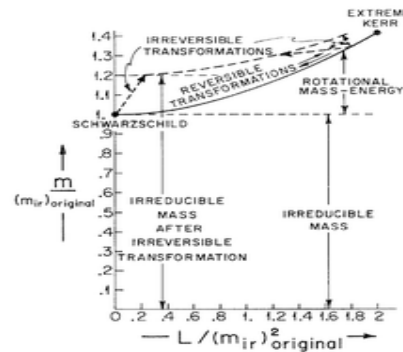

FIG. 1. Mass energy m versus angular momentum L for a black hole of specified irreducible mass m_{ir} illustrating the difference between reversible transformations and irreversible transformations (which increase the irreducible mass).
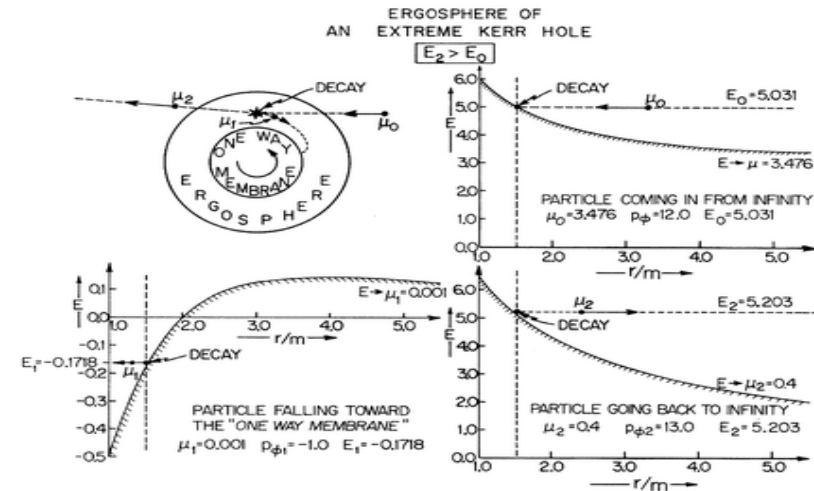

FIG. 2. (Reproduced from Ruffini and Wheeler, Ref. 4, with their kind permission.) Decay of a particle of rest-plus-kinetic energy E_0 into a particle which is captured into the black hole with positive energy as judged locally, but negative energy E_1 as judged from infinity, together with a particle of rest-plus-kinetic energy $E_2 > E_0$ which escapes to infinity. The cross-hatched curves give the effective potential (gravitational plus centrifugal) defined by the solution E of Eq. (2) for constant values of p_φ and μ.

equation[5] (where a is an abbreviation for L/m)

$$E^2[r^3 + a^2(r + 2m)] - 4mEap_\varphi + (2m-r)p_\varphi^2 - \mu^2 r^2(r-2m) - a^2\mu^2 r = \text{multiple of (radial momentum)}^2 = 0. \qquad (2)$$

The Penrose process is most efficient when the reduction of mass is greatest for a given reduction in angular momentum. To meet this requirement the energy E_1 must be as negative as possible. This happens at the surface of the black hole itself,

$$r = r_+ = m + (m^2 - a^2)^{1/2}, \qquad (3)$$

where the separation of "positive-" and negative-energy states goes to zero [vanishing of discriminant of Eq. (2) for E]. At this point the relation between energy and angular momentum reduces to

$$E_1 = [a/(r_+^2 + a^2)](p_\varphi)_1. \qquad (4)$$

Applying the laws of conservation of energy and angular momentum to the assimilation of particle 1 by the black hole, we arrive at the relation

$$dm = \frac{(L/m)\,dL}{[m + (m^2 - L^2/m^2)^{1/2}]^2 + L^2/m^2}. \qquad (5)$$

Integration leads to the relation

$$(1 - a^2/m^2)^{1/2} = (2m_{ir}^2/m^2)^{-1}$$

which, if condition (3) is fulfilled, is equivalent to expression (1).

I would like to thank Professor J. A. Wheeler and Dr. R. Ruffini for very helpful discussions and suggestions.

[1]J. Bardeen, "The Weight and Fate of a Relativistic Rotating Disk," relativity seminar, Princeton University, 5 May 1970 (unpublished).

[2]D. Christodoulou, Bull. Amer. Phys. Soc., **15**, 661 (1970).

[3]R. Penrose, Riv. Nuovo Cimento **1**, 252 (1969).

[4]R. Ruffini and J. A. Wheeler, in "The Significance of Space Research for Fundamental Physics" (European Space Research Organization, Paris, to be published).

[5]B. Carter, Phys. Rev. **174**, 1559 (1968).

Princeton, 1971

Joseph Henry Laboratories, Princeton University

Introducing the black hole

According to present cosmology, certain stars
end their careers in a total gravitational collapse that
transcends the ordinary laws of physics.

Remo Ruffini and John A. Wheeler

The quasistellar object, the pulsar, the neutron star have all come onto the scene of physics within the space of a few years. Is the next entrant destined to be the black hole? If so, it is difficult to think of any development that could be of greater significance. A black hole, whether of "ordinary size" (approximately one solar mass, $1\ M_\odot$), or much larger (around $10^8\ M_\odot$ to $10^{10}\ M_\odot$, as proposed in the nuclei of some galaxies) provides our "laboratory model" for the gravitational collapse, predicted by Einstein's theory, of the universe itself.

A black hole is what is left behind after an object has undergone complete gravitational collapse. Spacetime is so strongly curved that no light can come out, no matter can be ejected and no measuring rod can ever survive being put in. Any kind of object that falls into the black hole loses its separate identity, preserving only its mass, charge, angular momentum and linear momentum (see figure 1). No one has yet found a way to distinguish between two black holes constructed out of the most different kinds of matter if they have the same mass, charge and angular momentum. Measurement of these three determinants is permitted by their effect on the Kepler orbits of test objects, charged and uncharged, in revolution about the black hole.

How the physics of a black hole looks depends more upon an act of choice by the observer himself than an anything else. Suppose he decides to follow the collapsing matter through its collapse down into the black hole. Then he will see it crushed to indefi-

nitely high density, and he himself will be torn apart eventually by indefinitely increasing tidal forces. No restraining force whatsoever has the power to hold him away from this catastrophe, once he crossed a certain critical surface known as the "horizon." The final collapse occurs a finite time after the passage of this surface, but it is inevitable. Time and space are interchanged inside a black hole in an unusual way; the direction of increasing proper time for the observer is the direction of decreasing values of the coordinate r. The observer has no more power to return to a larger r value than he has power to turn back the hands on the clock of life itself. He can not even stay where he is, and for a simple reason: no one has the power to stop the advance of time.

Suppose the observer decides instead to observe the collapse from far away. Then, as price for his own safety, he is deprived of any chance to see more than the first steps on the way to collapse. All signals and all information from the later phases of collapse never escape; they are caught up in the collapse of the geometry itself.

That a sufficient mass of cold matter will necessarily collapse to a black hole (J. R. Oppenheimer and H. Snyder,[1] is one of the most spectacular of all the predictions of Einstein's standard 1915 general relativity. The geometry around a collapsed object of spherical symmetry (nonrotating!) was worked out by Karl Schwarzschild of Göttingen, father of the American astrophysicist Martin Schwarzschild, as early as 1916. In 1963 Roy Kerr[2] found the geometry associated with a rotating collapsed object. James Bardeen has recently emphasized that all stars have angular momentum and that most stars—or star cores—will have so much angular momentum that the black hole formed upon collapse will be rotating at the

Remo Ruffini and John Wheeler are both at Princeton University; Wheeler, currently on leave from Princeton, is spending a year at Cal Tech and Moscow State University.
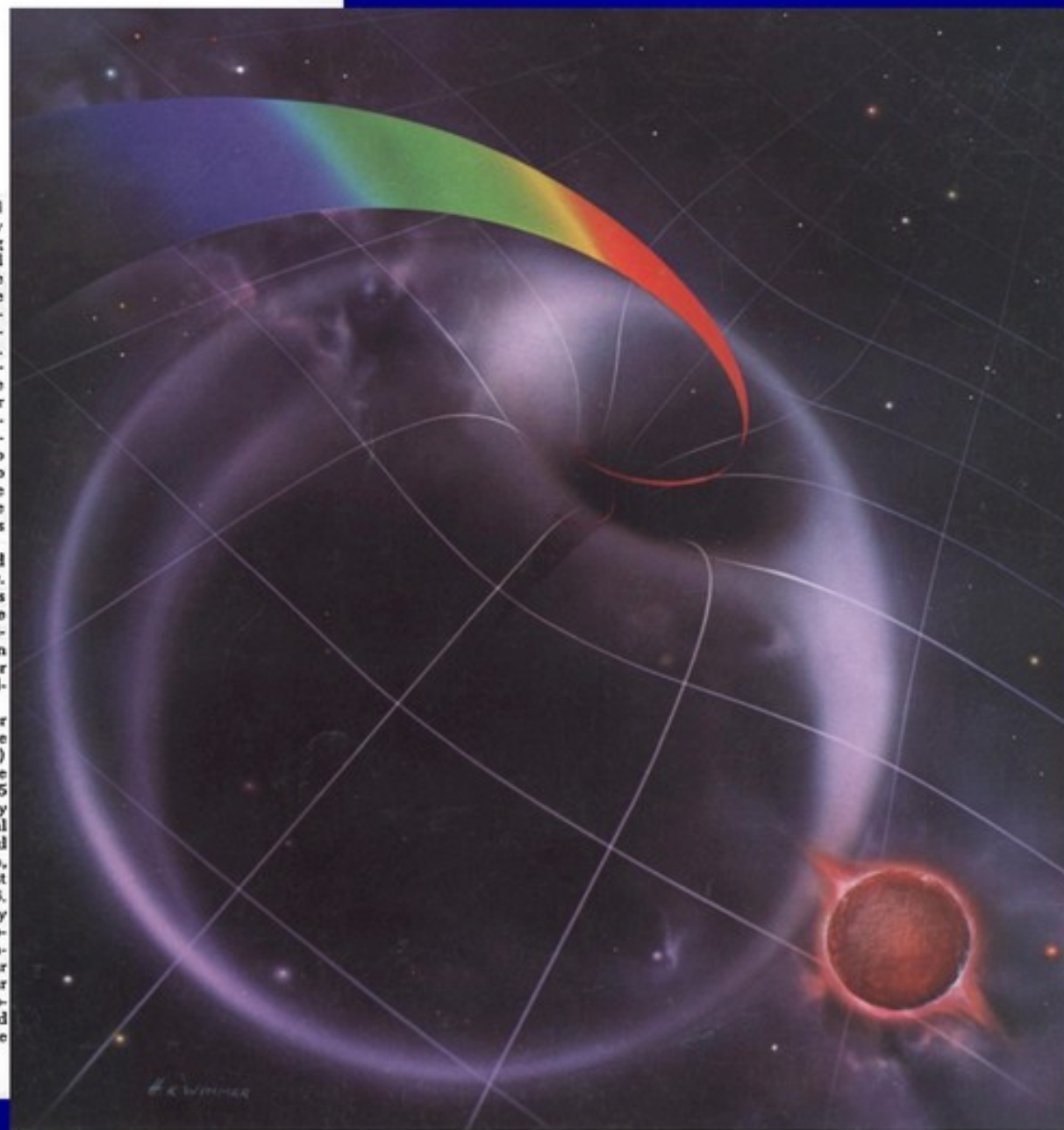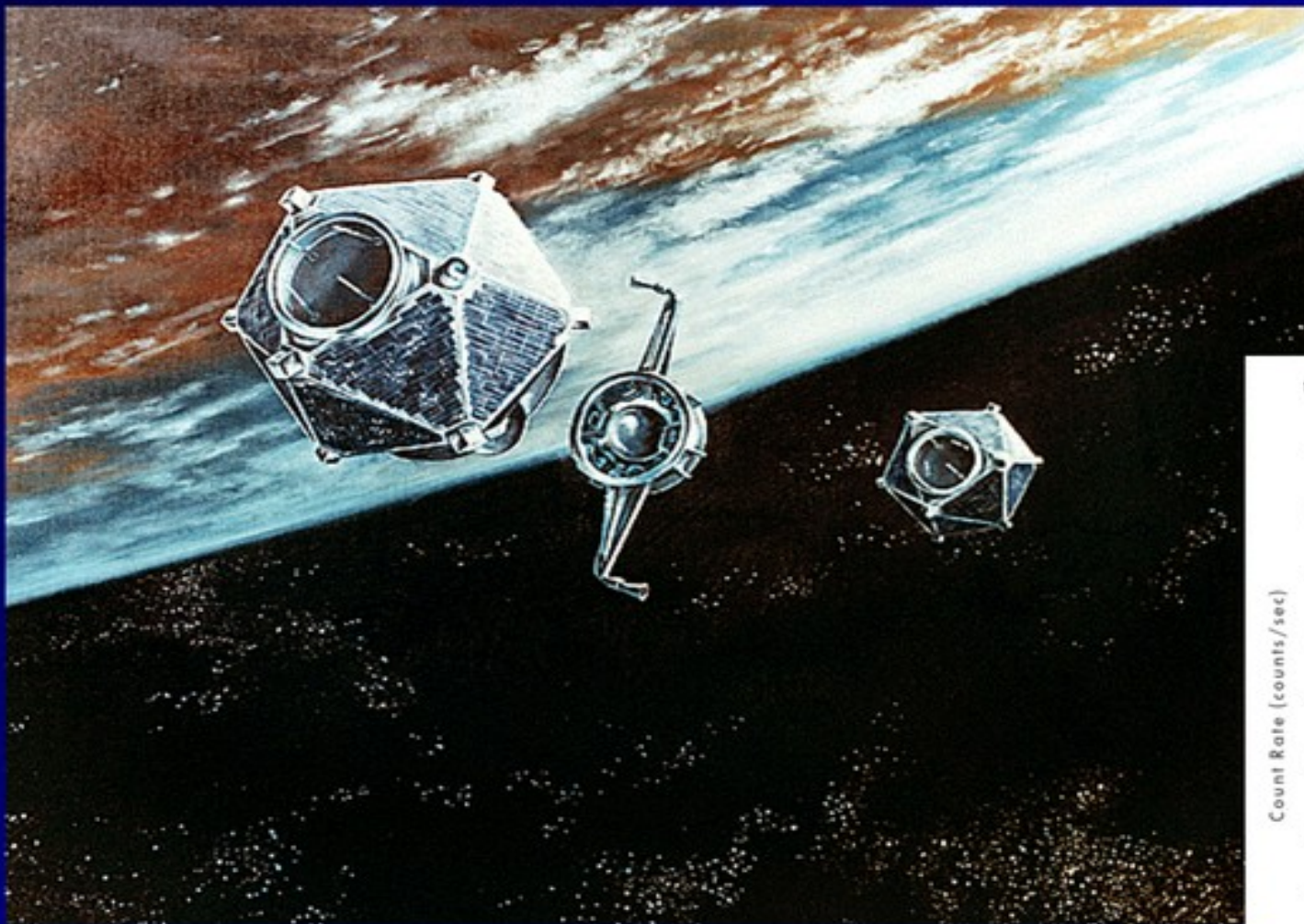
**Prof. Remo Ruffini and Prof. Roy Kerr
at Prof. Stephen Hawking's home in Cambridge
for dinner on June 20ᵗʰ, 2017**

Vela satellites and GRBs (60s-70s)

X-Ray: 3-12 keV
Gamma: 150-750 keV

R.W. Klebesadel, I.B. Strong, & R.A. Olson, ApJ Lett., 182, 1973
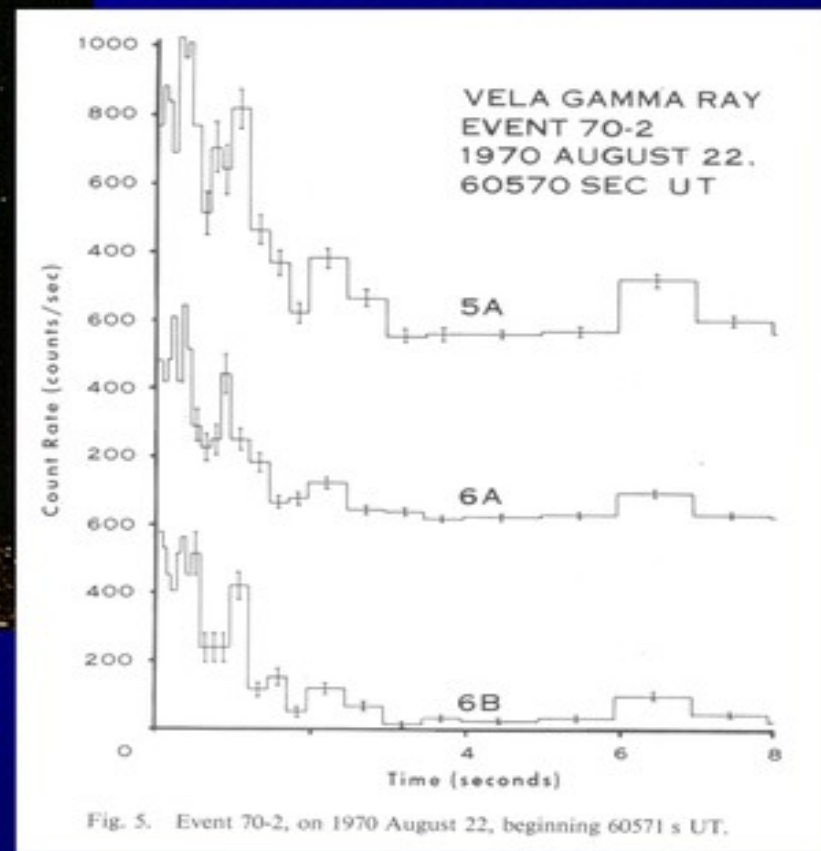
H. Gursky & R. Ruffini, AAAS, S. Francisco, 1974

VELA GAMMA RAY
EVENT 70-2
1970 AUGUST 22.
60570 SEC UT

Fig. 5. Event 70-2, on 1970 August 22, beginning 60571 s UT.

The new era: the launch of Beppo Sax on April 30, 1996

$E = 10^{54}$ erg

The Binary Nature of GRBs

The first successful proposal of relating a GRB to an astrophysical cosmological source came from the vision of Zoltan Paczynski and his school who identified the progenitors of short GRBs with merging binary NS (see, e.g., Paczynski 1986; Eichler et al. 1989; Narayan, Piran and Shemi 1991, 1992; Mao & Paczynski 1992; Narayan, Paczynski and Piran 1992). These results were later confirmed, after BeppoSAX, by Li & Paczynski (1998, 2000, 2006); see also the review by Berger (2014).

The traditional long GRBs model, as recalled in Zhang 2018, was introduced by Rees & Meszaros (1992); Mészáros & Rees (1997), and Woosley (1993) based on a single star, a BH, as the origin of GRBs emitting an ultrarelativistic blast wave with Lorentz Gamma Factor of $\sim10^3$ (Blandford & McKee 1976). The kinetic energy of such ultrarelativistic blast wave released by slowing down in the circumburst medium were assumed to give originate all GRBs emissions by synchroton at distances of 1016 - 1018 cm (Waxman & Piran 1994; Sari & Piran 1995; Sari et al. 1998).

In our approach we assume that all long GRBs, not only the short GRBs, originate from binary systems. These binaries are composed of different combinations of CO-stars, neutron stars (NS), white dwarfs (WD), black holes (BH) and new neutron stars νNS. Only in some of these subclasses the presence of a BH occurs (see e.g. Ruffini et al. 2016b, 2018a; Wang et al. 2019). Three subclasses are the BdHNe originating from a Co Core and the Companion NS binary, for selected binary periods. Each GRB emission originates generally from mildly relativistic process in specific and different GRB episodes.
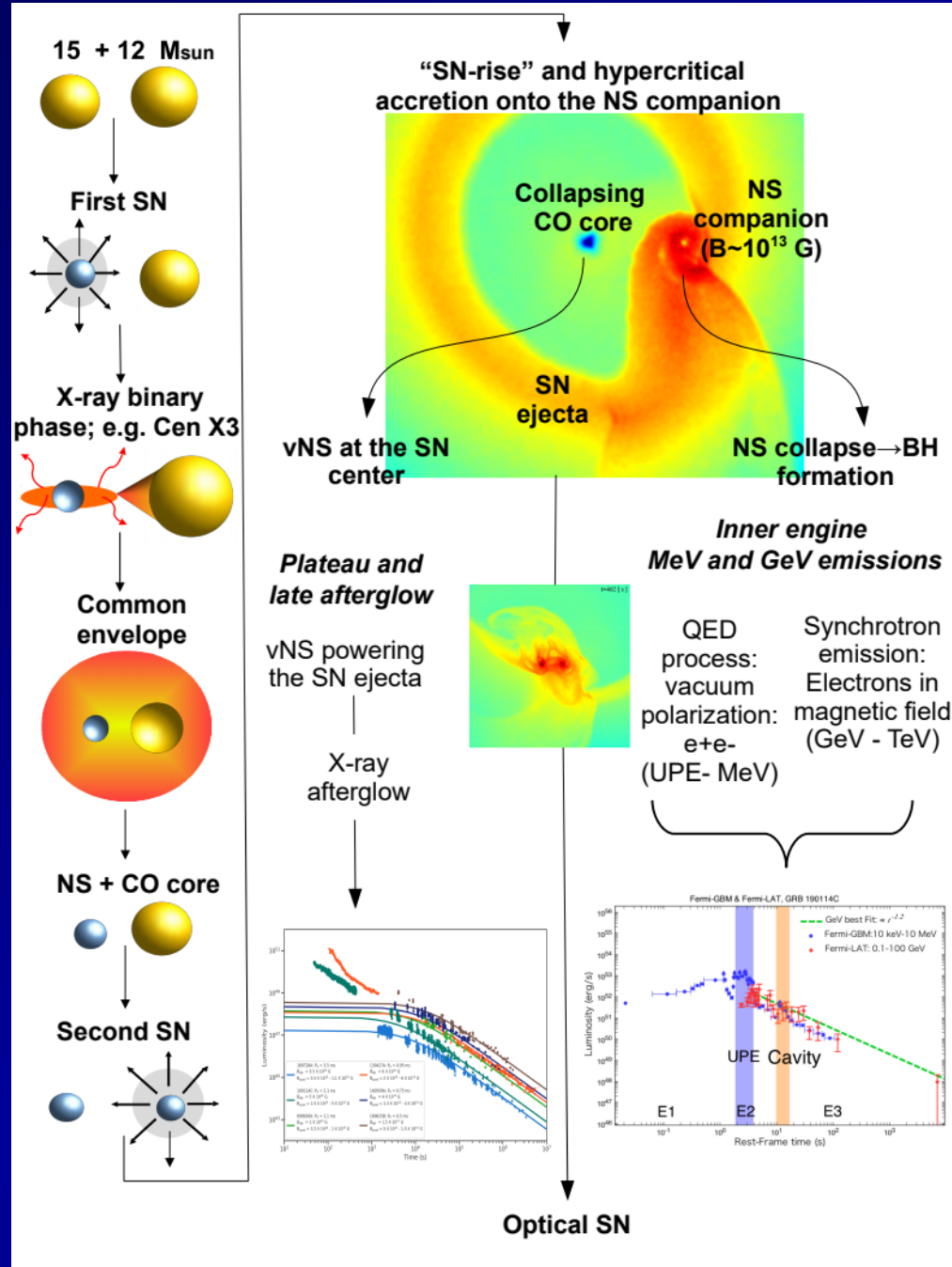
SATELLITE

## *Fermi Gamma-ray Space Telescope*

0
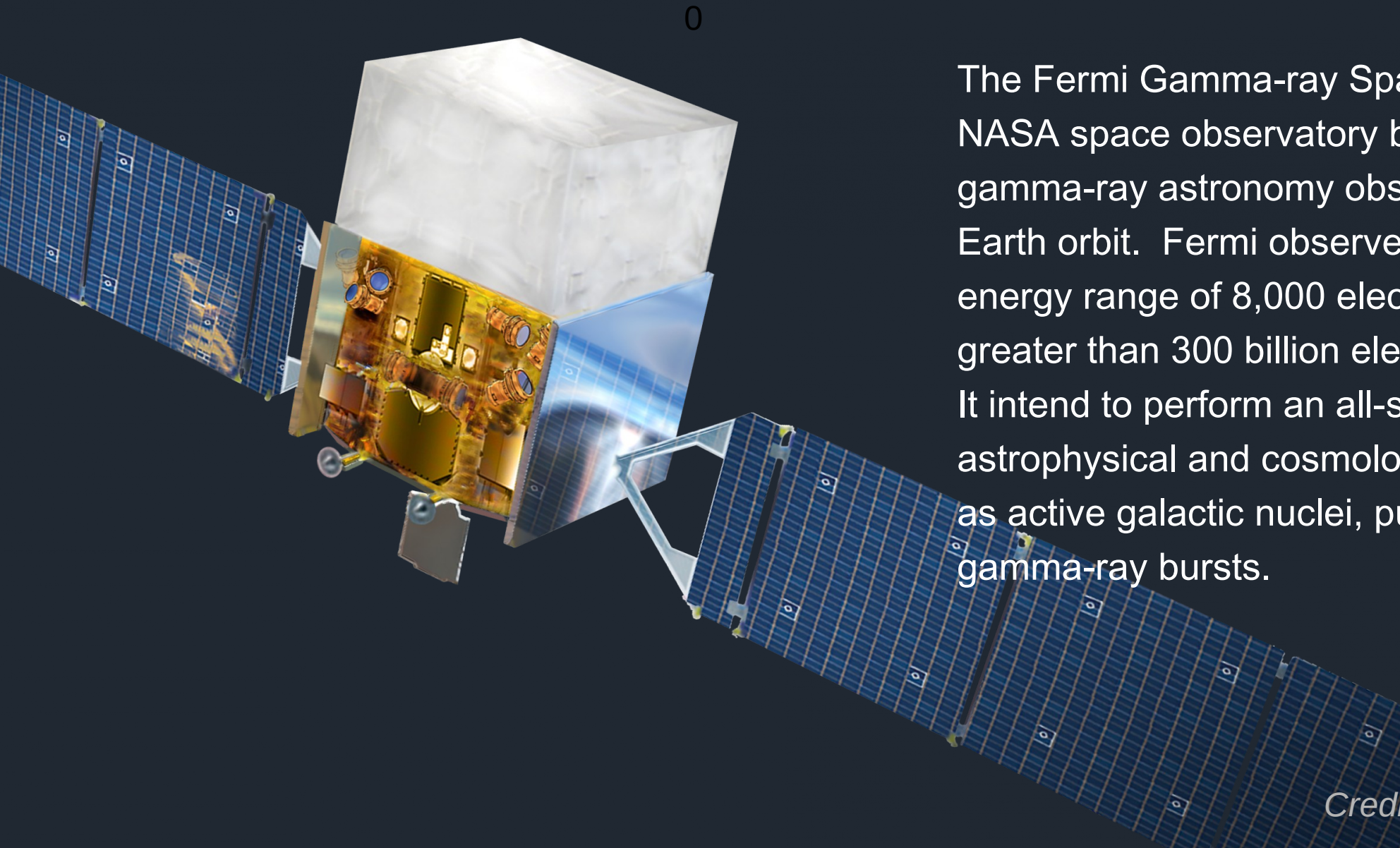
The Fermi Gamma-ray Space Telescope is a NASA space observatory being used to perform gamma-ray astronomy observations from low Earth orbit. Fermi observes light in the photon energy range of 8,000 electronvolts (8 keV) to greater than 300 billion electronvolts (300 GeV). It intend to perform an all-sky survey studying astrophysical and cosmological phenomena such as active galactic nuclei, pulsars, dark matter, and gamma-ray bursts.

Credit: NASA, Wikipedia
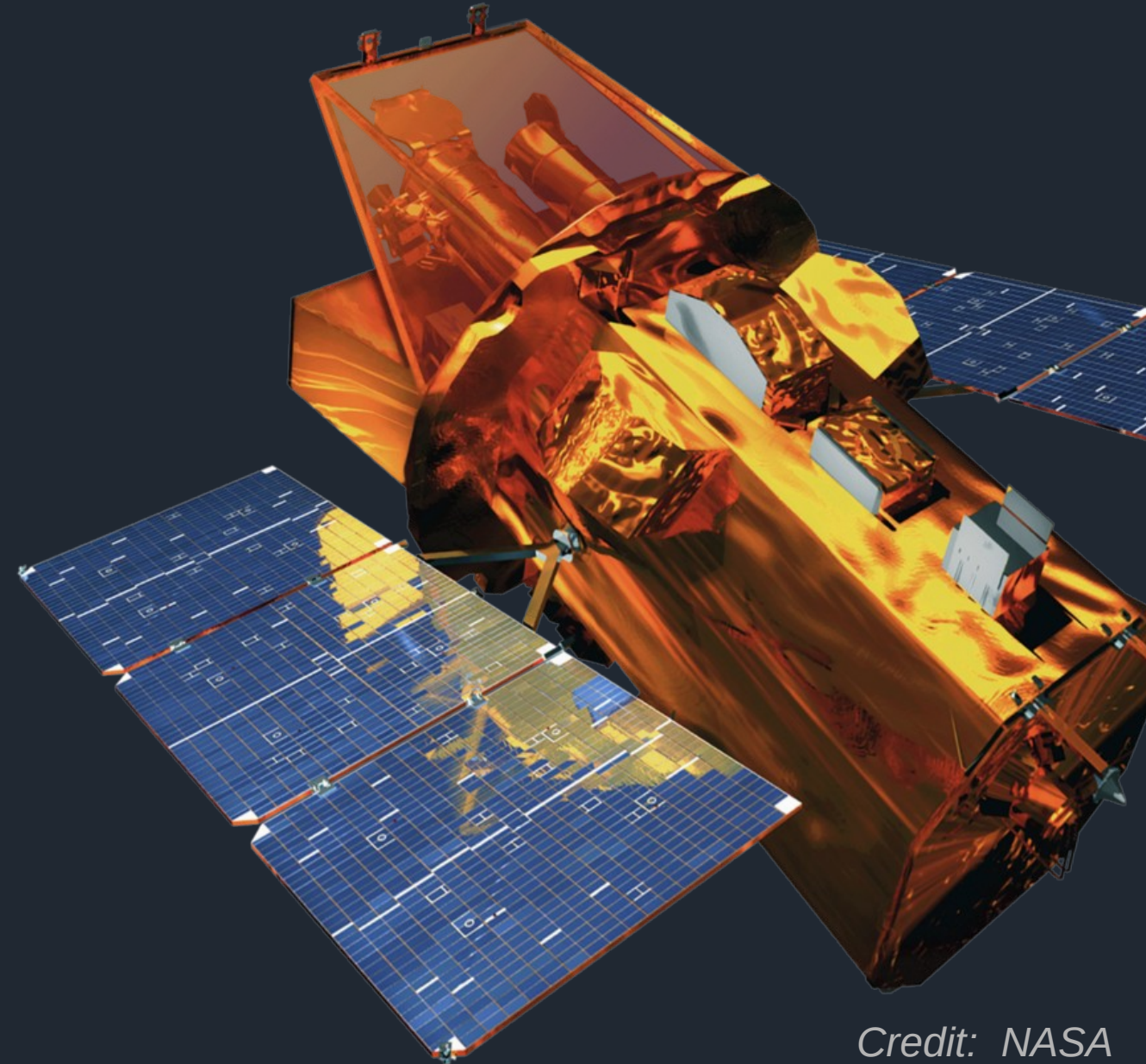
TELESCOPE
Very Large Telescope (VLT)

The Very Large Telescope array (VLT) is the flagship facility for European ground-based astronomy at the beginning of the third Millennium. It is the world's most advanced optical instrument consisting of four Unit Telescopes with main mirrors of 8.2m diameter and four movable 1.8m diameter Auxiliary Telescopes.
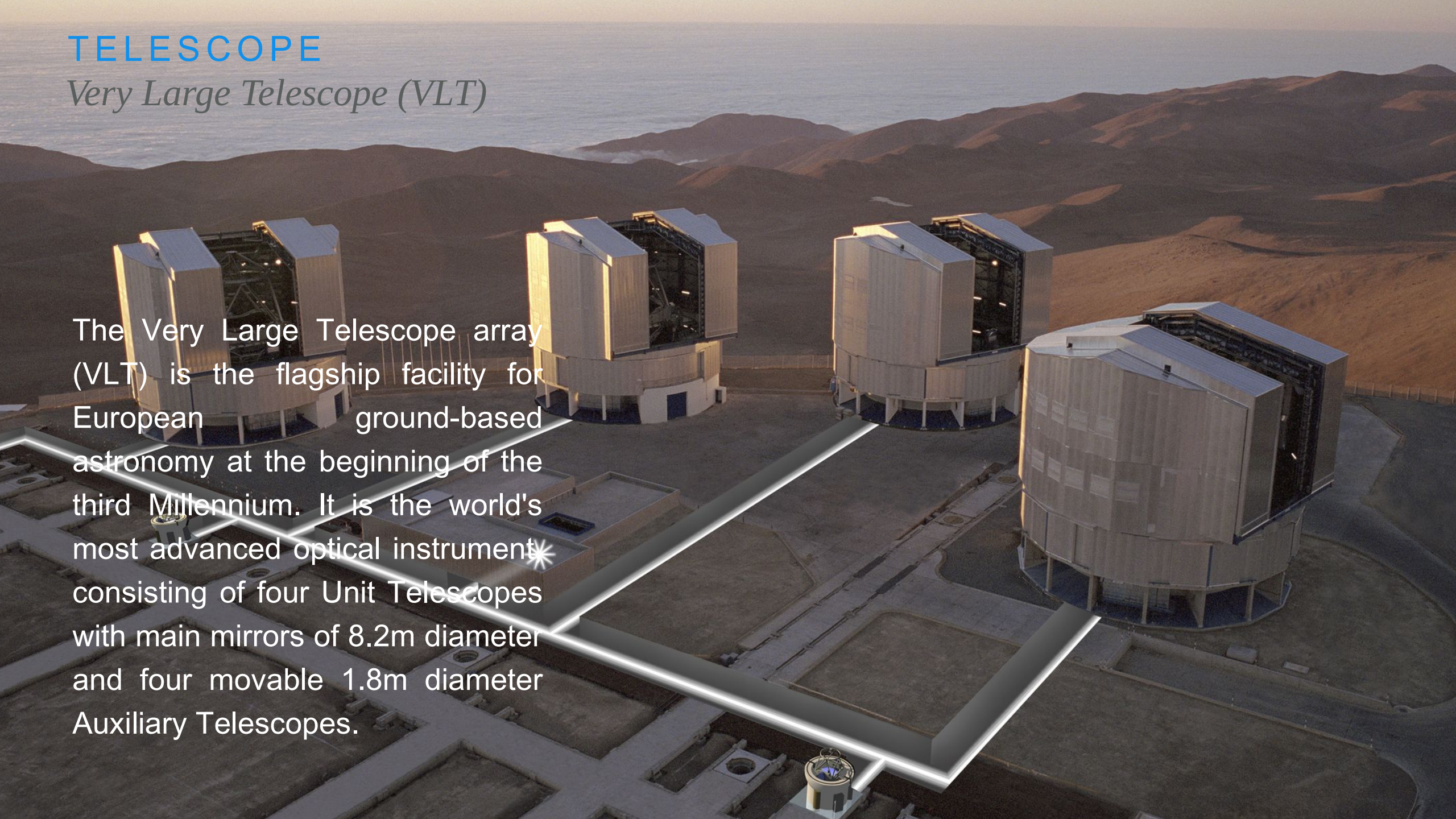
SATELLITE
Neil Gehrels Swift Observatory

Swift is NASA space satellite. It is the first multi-wavelength observatory dedicated to the study of gamma-ray-burst (GRB) science. Its three instruments work together to observe GRBs and afterglows in the gamma-ray, X-ray, ultraviolet, and optical wavebands. Swift monitors the sky for new GRBs with a wide-field detector, localizes their positions onboard, and autonomously reorients itself to observe the new burst quickly with its other telescopes.

Credit: NASA

TELESCOPE

Major Atmospheric Gamma Imaging Cherenkov telescope (MAGIC)

MAGIC (Major Atmospheric Gamma Imaging Cherenkov Telescopes) is a system of two Imaging Atmospheric Cherenkov telescopes situated at the Roque de los Muchachos Observatory on La Palma, one of the Canary Islands, at about 2200 m above sea level. MAGIC is a system of two 17m diameter, F/1.03 Imaging Atmospheric Cherenkov Telescopes (IACT). They are dedicated to the observation of gamma rays from galactic and extragalactic sources in the very high energy range (VHE, 30 GeV to 100 TeV).

Hard X-ray Modulation Telescope (HXMT)

The Hard X-ray Modulation Telescope (HXMT) , named "Insight", is China's first X-ray astronomy satellite. There are three main payloads onboard Insight-HXMT, the high energy X-ray telescope (20-250 keV, 5100 cm2), the medium energy X-ray telescope (5-30 keV, 952 cm2), and the low energy X-ray telescope (1-15 keV, 384 cm2). The main scientific objectives of Insight-HXMT are: (1) to scan the Galactic Plane to find new transient sources and to monitor the known variable sources, (2) to observe X-ray binaries to study the dynamics and emission mechanism in strong gravitational or magnetic fields, and (3) to find and study gamma-ray bursts with its anti-coincidence CsI detectors.

On 14 January, 2019, *Fermi*-GBM was triggered by GRB 190114C (Hamburg et al. 2019). Following 0.37 s the *Neil Gehrels Swift* Burst Alert Telescope (BAT) was also triggered (J.D. Gropp et al. 2019). Its distance (redshift $z = 0.42$) was determined a few hours later by the Nordic Optical Telescope (J. Selsing et al. 2019). On January 15, 2019, solely on the ground of the above observations, we recognized that this source was a BdHN I (Ruffini et al. 2019d), anticipating the possibility of the appearance of an associated supernova (SN). The SN was detected at the predicted time by A. Melandri et al. (2019).
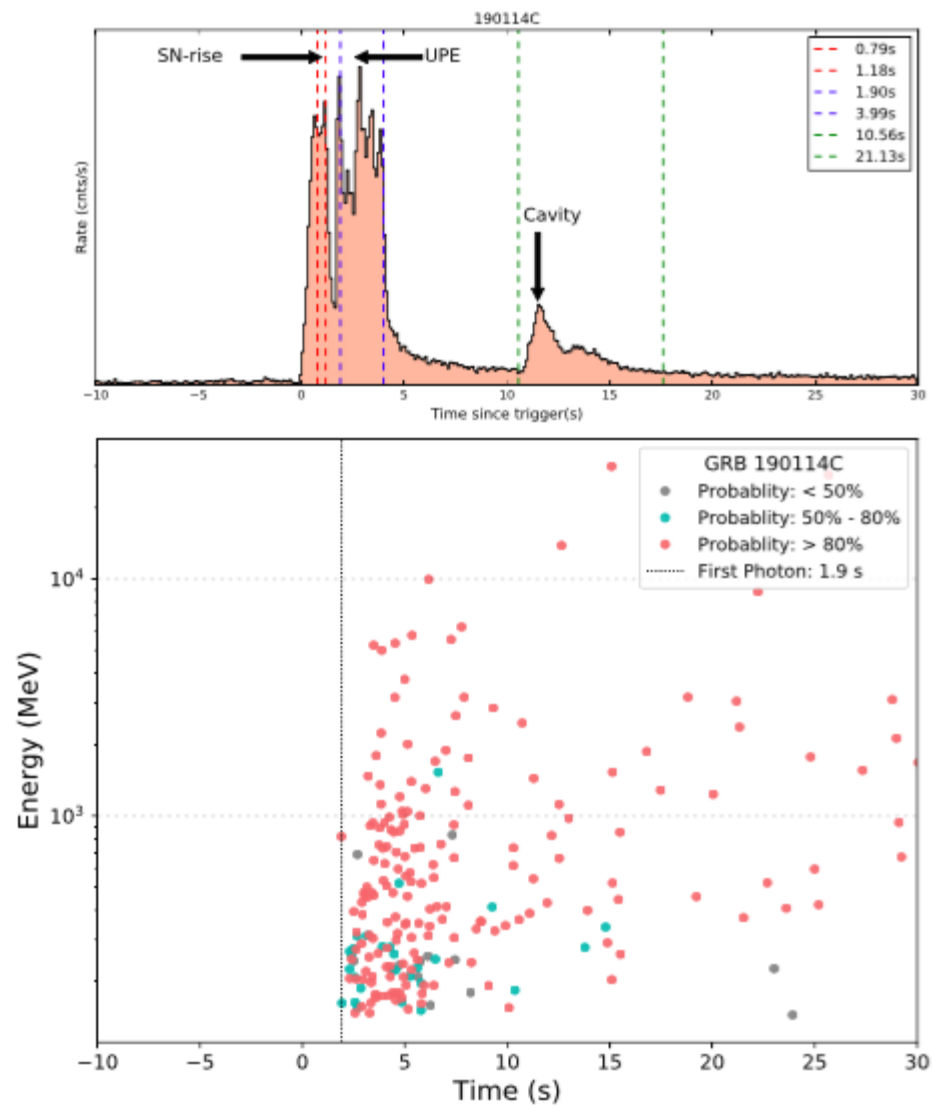
Fig. 4. The onset of the GeV radiation coincides with the onset of the UPE. **Upper**: the properties of the prompt emission of GRB 190114C in the rest frame, the UPE phase starts at $t_{rf} = 1.9$ s in the rest-frame. **Lower**: the arrival time of Fermi-LAT photons in the energy band of 0.1–20 GeV, the first photon arrives at $t_{rf} = 1.9$ s as indicated by a vertical dotted line.
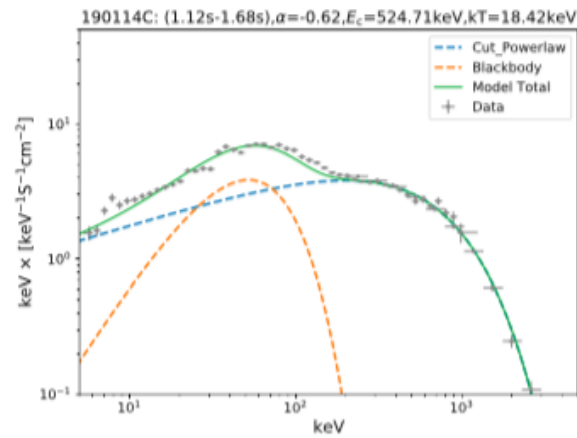
Spectrum of SN-rise
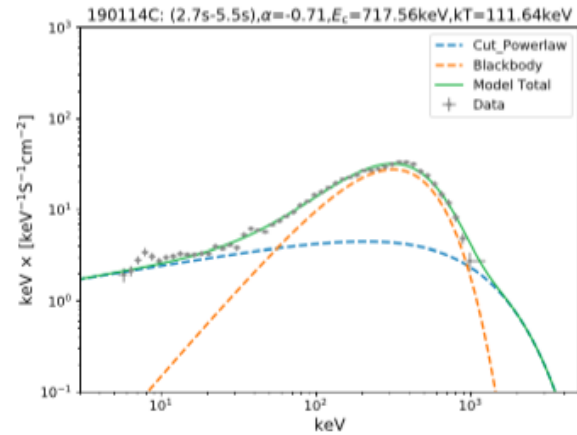
Spectrum of UPE phase
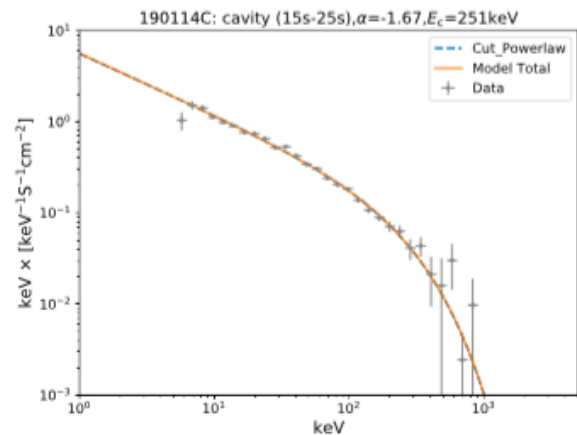
Spectrum of Cavity

The Papapetrou Wald Solution

Fig. 13. The electromagnetic field lines of the Wald solution. The red lines show the magnetic field lines and the blue show the electric field lines. The Magnetic field is "parallel" to the spin of the Kerr BH, so parallel to the rotation axis. On the polar axis up to $\theta \sim \pi/3$ electric field lines are inwardly directed, therefore electrons are accelerated away from the BH. For $\theta > \pi/3$ electric field lines are outwardly directed and consequently protons are accelerated away from the BH.

Details in Ruffini et al. ApJ 886 (2019) 82

$$E_{\hat{r}} = \frac{\hat{a}B_0}{\Sigma}\left[r\sin^2\theta - \frac{\hat{M}\left(\cos^2\theta + 1\right)\left(r^2 - \hat{a}^2\cos^2\theta\right)}{\Sigma}\right], \quad (29)$$

$$E_{\hat{\theta}} = \frac{\hat{a}B_0}{\Sigma}\sin\theta\cos\theta\sqrt{\Delta}, \quad (30)$$

$$B_{\hat{r}} = -\frac{B_0\cos\theta\left(-\frac{2\hat{a}^2\hat{M}r\left(\cos^2\theta+1\right)}{\Sigma} + \hat{a}^2 + r^2\right)}{\Sigma}, \quad (31)$$

$$B_{\hat{\theta}} = \frac{B_0 r}{\Sigma}\sin\theta\sqrt{\Delta}, \quad (32)$$

where $\Sigma = r^2 + \hat{a}^2\cos^2\theta$ and $\Delta = r^2 - 2\hat{M}r + \hat{a}^2$, being $\hat{M} = GM/c^2$ and $\hat{a} = a/c = J/(M c)$. The (outer) event horizon is located at $r_+ = (G/c^2)(\hat{M} + \sqrt{\hat{M}^2 - \hat{a}^2})$.

For simplicity, we evaluate the field in the polar direction $\theta = 0$:

$$E_{\hat{r}} = -\frac{2B_0 J G}{c^3}\frac{\left(r^2 - \hat{a}^2\right)}{\left(r^2 + \hat{a}^2\right)^2} \quad (33)$$

$$E_{\hat{\theta}} = 0 \quad (34)$$

$$B_{\hat{r}} = \frac{B_0\left(-\frac{4G J^2 r}{M\left(r^2 + \hat{a}^2\right)} + a^2 + r^2\right)}{\left(r^2 + \hat{a}^2\right)} \quad (35)$$

$$B_{\hat{\theta}} = 0. \quad (36)$$

considering an equivalent charge as

$$Q_{\text{eff}} = 2B_0 J G/c^3 \quad (37)$$

The radial component of the electric field can be approximated by the expression

$$E_{\hat{r}} = -\frac{2B_0 J G}{c^3}\frac{\left(r^2 - \hat{a}^2\right)}{\left(r^2 + \hat{a}^2\right)^2} \approx -\frac{1}{2}\alpha B_0\frac{r_+^2}{r^2}. \quad (38)$$

For spin values $\alpha \lesssim 0.7$, the electric energy is well approximated by (Ruffini et al. 2019c)

$$\mathcal{E} \approx \frac{Q_{\text{eff}}^2}{2 r_+} = 1.25 \times 10^{43}\frac{\beta^2\alpha^2\mu^3}{1 + \sqrt{1 - \alpha^2}}\text{ erg}, \quad (39)$$

where we have introduced the notation $\mu = M/M_\odot$ and $\beta = B_0/B_c$, with

$$B_c = E_c = \frac{m_e^2 c^3}{e\hbar}, \quad (40)$$

the critical field for vacuum polarization.

The "blackholic quantum" of energy

Table 1 *Inner engine* astrophysical quantities for GRBs and AGN. The power reported in the last row is the one to accelerate ultrahigh-energy particles, i.e. $\dot{\mathcal{E}} = \mathcal{E}/\tau_{\text{el}}$. In both cases the parameters (mass, spin and magnetic field) have been fixed to explain the observed high-energy ($\gtrsim$ GeV) luminosity

	GRB (130427-like)	AGN (M87*-like)
τ_{el}	2.21×10^{-5} s	0.49 day
ε_e (eV)	1.68×10^{18}	1.19×10^{19}
$\mathcal{E}$ (erg)	4.73×10^{36}	5.19×10^{47}
$\dot{\mathcal{E}}$ (erg/s)	2.21×10^{41}	1.22×10^{43}

Along BH rotation axis:
ultrahigh-energy cosmic rays (UHECRs)

Rueda & Ruffini; EPJC 80, 300 (2020); arXiv:1907.08066
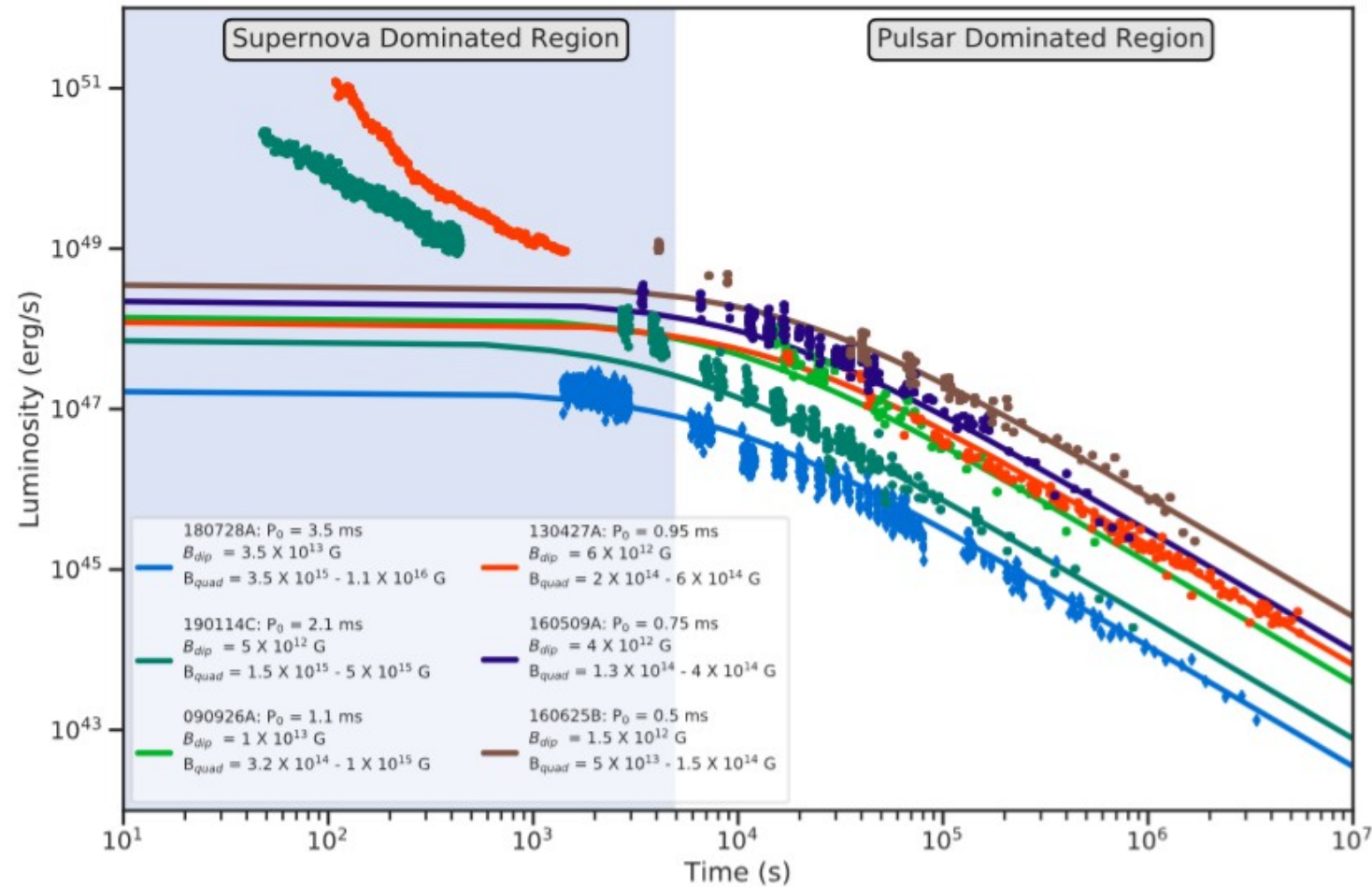
Figure 5. The brown, deep blue, orange, green and bright blue points correspond to the bolometric (about $\sim$ 5 times brighter than the soft X-ray observed by Swift-XRT inferred from the fitted sychrotron spectrum) light curves of GRB 160625B, 160509A, 130427A, 190114C and 180728A, respectively. The lines are the fitting of the energy injection from the rotational energy of the pulsar. The pulsar powers the late afterglow ($t \gtrsim 5 \times 10^{3}$ s, white background), while in the earlier time ($t \lesssim 5 \times 10^{3}$ s, dusty blue background), the remaining kinectic energy of the SN ejecta plays the leading role.

J. A. Rueda et al 2020 ApJ 893 148
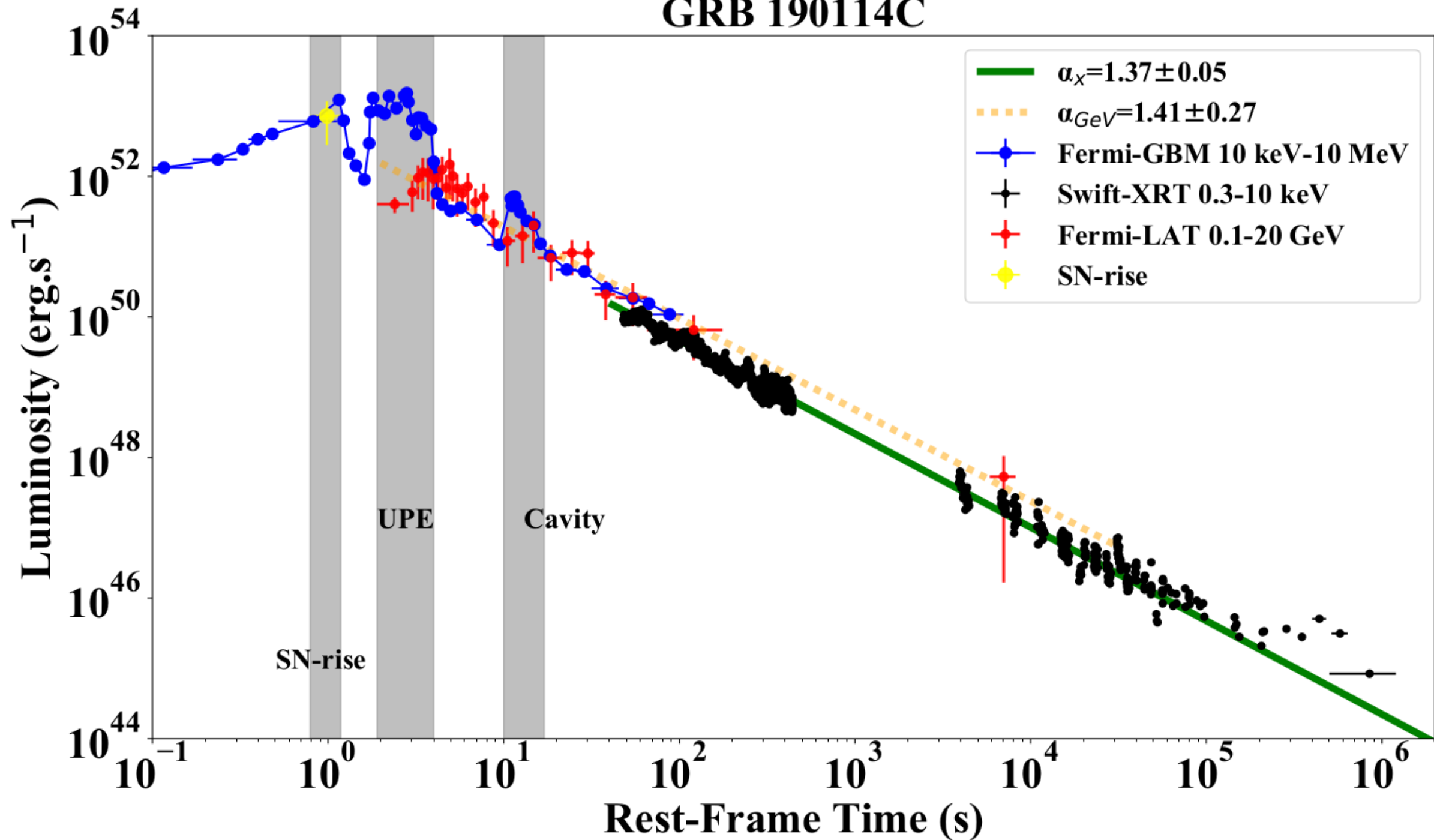
GRB 190114C

Time-resolved analysis of GRB 190114C_ UPE phase

Table 1. Results of the time-resolved spectral fits of GRB 190114C (CPL+BB model) from $t = 2.7$ s ($t_{rf} = 1.9$ s) to $t = 5.5$ s ($t_{rf} = 3.99$ s). The time intervals both in the rest-frame and observer's frame, the significance (S) for each time interval, the power-law index, rest-frame cut-off energy, rest-frame temperature, AIC/BIC, BB flux, total flux, the ratio of blackbody flux to the total flux, F_{BB}/F_{tot} and finally the isotropic energy are reported in this table. The F_{BB}/F_{tot} remains almost constant in each sample. The Akaike Information Criterion (AIC, Akaike 1974) and the Bayesian Information Criterion (BIC, Schwarz et al. 1978) can be used to select non-nested and nested models, respectively. The AIC and BIC are defined as AIC$=-2\ln L(\theta)+2k$ and BIC$=-2\ln L(\theta)+k\ln(n)$, respectively. Here L is the maximized value of the likelihood function for the estimated model, k is the number of free parameters to be estimated, n is the number of observations (or the sample size). The prefer model between any two estimated models is the one that provides the minimum AIC and BIC scores. After comparing the AIC and BIC, we find the CPL+BB model is the preferred model than the CPL and other model. The likelihood -log(posterior) and the AIC and BIC scores are reported in column 6.

$t_1 \sim t_2$ (s) Obs	$t_{rf,1} \sim t_{rf,2}$ (s) Rest-frame	S	α	E_c (keV)	kT (keV)	ΔDIC	F_{BB} (10^{-6}) (erg cm^{-2} s^{-1})	F_{tot} (10^{-6}) (erg cm^{-2} s^{-1})	F_{ratio}	E_{tot} (erg)
2.700~5.500	1.896~3.862	418.62	$-0.71^{+0.02}_{-0.02}$	$717.6^{+25.4}_{-25.4}$	$159.0^{+3.6}_{-3.6}$	-3344/6697/6719	$22.49^{+3.21}_{-2.65}$	$111.10^{+11.60}_{-10.40}$	0.20	1.50e+53
2.700~4.100	1.896~2.879	296.60	$-0.51^{+0.02}_{-0.02}$	$696.6^{+31.9}_{-32.4}$	$209.7^{+9.3}_{-9.1}$	-2675/5360/5381	$24.67^{+6.93}_{-5.35}$	$142.50^{+23.90}_{-21.00}$	0.17	9.64e+52
4.100~5.500	2.879~3.862	318.07	$-0.90^{+0.02}_{-0.02}$	$639.3^{+31.9}_{-31.6}$	$130.6^{+2.5}_{-2.5}$	-2529/5069/5090	$25.55^{+2.97}_{-2.75}$	$80.98^{+9.68}_{-8.07}$	0.32	5.48e+52
2.700~3.400	1.896~2.388	204.30	$-0.59^{+0.03}_{-0.03}$	$724.7^{+44.5}_{-45.5}$	$220.0^{+17.1}_{-17.2}$	-1882/3774/3796	$18.55^{+9.42}_{-7.40}$	$123.90^{+29.20}_{-22.30}$	0.15	4.19e+52
3.400~4.100	2.388~2.879	225.88	$-0.46^{+0.04}_{-0.03}$	$699.8^{+47.8}_{-48.3}$	$196.7^{+8.9}_{-8.7}$	-2032/4074/4095	$31.78^{+9.60}_{-7.31}$	$161.40^{+47.10}_{-32.40}$	0.20	5.46e+52
4.100~4.800	2.879~3.371	233.97	$-0.84^{+0.04}_{-0.03}$	$608.1^{+42.1}_{-42.7}$	$130.4^{+3.7}_{-3.9}$	-1880/3770/3792	$23.94^{+4.20}_{-4.22}$	$85.37^{+14.83}_{-12.27}$	0.28	2.89e+52
4.800~5.500	3.371~3.862	227.90	$-0.96^{+0.03}_{-0.03}$	$679.5^{+49.1}_{-48.7}$	$130.6^{+3.1}_{-3.7}$	-1809/3628/3649	$27.18^{+4.01}_{-3.73}$	$78.20^{+11.40}_{-9.66}$	0.35	2.65e+52
2.700~3.050	1.896~2.142	148.59	$-0.59^{+0.03}_{-0.03}$	$547.7^{+44.2}_{-44.9}$	$240.8^{+29.2}_{-29.1}$	-1187/2384/2406	$19.67^{+17.96}_{-8.88}$	$103.20^{+30.60}_{-20.28}$	0.19	1.75e+52
3.050~3.400	2.142~2.388	145.04	$-0.60^{+0.03}_{-0.03}$	$965.2^{+28.5}_{-30.4}$	$203.5^{+14.8}_{-14.8}$	-1320/2650/2671	$22.87^{+8.88}_{-7.23}$	$152.00^{+24.00}_{-21.00}$	0.15	2.57e+52
3.400~3.750	2.388~2.633	134.60	$-0.63^{+0.04}_{-0.04}$	$885.7^{+70.9}_{-70.1}$	$240.6^{+10.5}_{-10.6}$	-1224/2458/2480	$41.02^{+11.09}_{-7.91}$	$129.10^{+32.40}_{-23.40}$	0.32	2.18e+52
3.750~4.100	2.633~2.879	187.77	$-0.35^{+0.06}_{-0.04}$	$607.8^{+57.1}_{-60.1}$	$151.5^{+12.4}_{-14.2}$	-1428/2866/2887	$23.92^{+12.46}_{-10.40}$	$192.00^{+101.70}_{-60.30}$	0.12	3.25e+52
4.100~4.450	2.879~3.125	171.81	$-0.69^{+0.05}_{-0.04}$	$515.9^{+43.6}_{-43.6}$	$117.3^{+5.0}_{-5.0}$	-1271/2552/2573	$19.19^{+4.89}_{-4.40}$	$92.71^{+27.69}_{-22.43}$	0.21	1.57e+52
4.450~4.800	3.125~3.371	230.14	$-0.98^{+0.04}_{-0.04}$	$702.0^{+78.1}_{-78.2}$	$141.3^{+5.8}_{-5.8}$	-1254/2518/2539	$26.76^{+6.41}_{-5.47}$	$80.73^{+17.95}_{-14.95}$	0.33	1.37e+52
4.800~5.150	3.371~3.617	166.30	$-0.97^{+0.04}_{-0.04}$	$685.1^{+69.4}_{-68.6}$	$140.8^{+4.6}_{-4.6}$	-1218/2447/2468	$31.83^{+6.85}_{-4.98}$	$82.51^{+15.62}_{-12.33}$	0.39	1.40e+52
5.150~5.500	3.617~3.862	161.51	$-0.95^{+0.04}_{-0.04}$	$692.2^{+79.1}_{-77.7}$	$120.0^{+4.0}_{-4.0}$	-1203/2416/2438	$23.19^{+5.38}_{-3.81}$	$73.57^{+18.69}_{-12.93}$	0.32	1.24e+52
2.700~2.875	1.896~2.019	117.09	$-0.58^{+0.05}_{-0.05}$	$470.5^{+74.4}_{-83.7}$	$261.5^{+29.0}_{-27.9}$	-640/1291/1311	$33.68^{+20.39}_{-14.33}$	$112.30^{+28.37}_{-25.73}$	0.30	9.50e+51
2.875~3.050	2.019~2.142	94.40	$-0.68^{+0.05}_{-0.05}$	$627.6^{+87.0}_{-91.5}$	$258.0^{+30.1}_{-28.7}$	-664/1337/1359	$28.45^{+20.42}_{-12.51}$	$98.14^{+33.56}_{-26.44}$	0.29	8.30e+51
3.050~3.225	2.142~2.265	106.62	$-0.59^{+0.05}_{-0.03}$	$957.1^{+34.1}_{-34.9}$	$245.3^{+21.5}_{-21.0}$	-768/1547/1568	$25.71^{+13.87}_{-9.03}$	$169.30^{+38.20}_{-31.60}$	0.15	1.43e+52
3.225~3.400	2.265~2.388	100.40	$-0.73^{+0.06}_{-0.05}$	$1275.9^{+208.9}_{-215.4}$	$208.6^{+9.1}_{-9.2}$	-669/1349/1369	$36.78^{+9.54}_{-8.93}$	$144.90^{+33.02}_{-27.63}$	0.25	1.23e+52
3.400~3.575	2.388~2.511	98.23	$-0.59^{+0.06}_{-0.05}$	$804.0^{+86.7}_{-82.3}$	$255.9^{+17.4}_{-17.4}$	-702/1414/1436	$42.19^{+19.41}_{-13.59}$	$139.30^{+48.30}_{-35.60}$	0.30	1.18e+52
3.575~3.750	2.511~2.633	93.84	$-0.65^{+0.04}_{-0.05}$	$916.3^{+64.6}_{-67.7}$	$229.3^{+13.6}_{-13.5}$	-730/1471/1492	$39.25^{+11.97}_{-10.21}$	$119.50^{+32.90}_{-25.45}$	0.33	1.01e+52
3.750~3.925	2.633~2.756	126.63	$-0.51^{+0.04}_{-0.02}$	$960.9^{+30.9}_{-31.4}$	$204.6^{+9.9}_{-10.0}$	-808/1627/1648	$57.70^{+19.81}_{-16.25}$	$221.10^{+35.60}_{-31.60}$	0.26	1.87e+52
3.925~4.100	2.756~2.879	141.61	$-0.27^{+0.06}_{-0.05}$	$412.7^{+12.2}_{-11.9}$	$196.8^{+14.0}_{-16.1}$	-729/1468/1488	$32.20^{+19.05}_{-18.86}$	$176.50^{+12.91}_{-11.21}$	0.18	1.49e+52
4.100~4.275	2.879~3.002	122.91	$-0.54^{+0.06}_{-0.08}$	$474.1^{+45.5}_{-46.9}$	$162.6^{+14.9}_{-14.8}$	-758/1526/1547	$24.26^{+17.09}_{-9.09}$	$116.10^{+52.40}_{-35.12}$	0.21	9.82e+51
4.275~4.450	3.002~3.125	122.62	$-0.64^{+0.06}_{-0.08}$	$365.0^{+44.9}_{-48.5}$	$107.5^{+15.7}_{-12.6}$	-675/1360/1380	$9.04^{+9.47}_{-5.69}$	$72.20^{+19.06}_{-14.95}$	0.13	6.11e+51
4.450~4.625	3.125~3.248	111.94	$-1.04^{+0.05}_{-0.05}$	$640.0^{+108.7}_{-106.1}$	$161.0^{+11.1}_{-10.8}$	-640/1290/1310	$22.34^{+9.36}_{-6.65}$	$68.54^{+11.70}_{-11.34}$	0.33	5.80e+51
4.625~4.800	3.248~3.371	123.33	$-0.95^{+0.05}_{-0.05}$	$694.2^{+96.8}_{-94.2}$	$146.3^{+6.7}_{-6.6}$	-734/1477/1499	$35.59^{+9.47}_{-8.00}$	$89.91^{+27.59}_{-18.82}$	0.40	7.60e+51
4.800~4.975	3.371~3.494	129.65	$-0.85^{+0.05}_{-0.03}$	$564.5^{+68.9}_{-71.9}$	$135.3^{+7.5}_{-7.6}$	-744/1498/1519	$30.78^{+11.12}_{-8.55}$	$96.58^{+31.02}_{-23.68}$	0.32	8.17e+51
4.975~5.150	3.494~3.617	107.36	$-1.10^{+0.04}_{-0.04}$	$820.5^{+115.0}_{-115.8}$	$149.7^{+5.9}_{-5.8}$	-683/1376/1398	$32.76^{+6.98}_{-5.92}$	$71.57^{+16.74}_{-11.99}$	0.46	6.05e+51
5.150~5.325	3.617~3.739	108.96	$-1.04^{+0.05}_{-0.05}$	$765.2^{+119.0}_{-115.8}$	$130.9^{+5.8}_{-5.8}$	-697/1404/1426	$26.14^{+7.02}_{-5.96}$	$66.70^{+20.48}_{-14.17}$	0.39	5.64e+51
5.325~5.500	3.739~3.862	121.57	$-0.88^{+0.06}_{-0.06}$	$635.3^{+88.7}_{-92.0}$	$108.9^{+5.3}_{-5.4}$	-736/1483/1504	$20.90^{+6.51}_{-5.15}$	$79.48^{+28.02}_{-21.03}$	0.26	6.72e+51
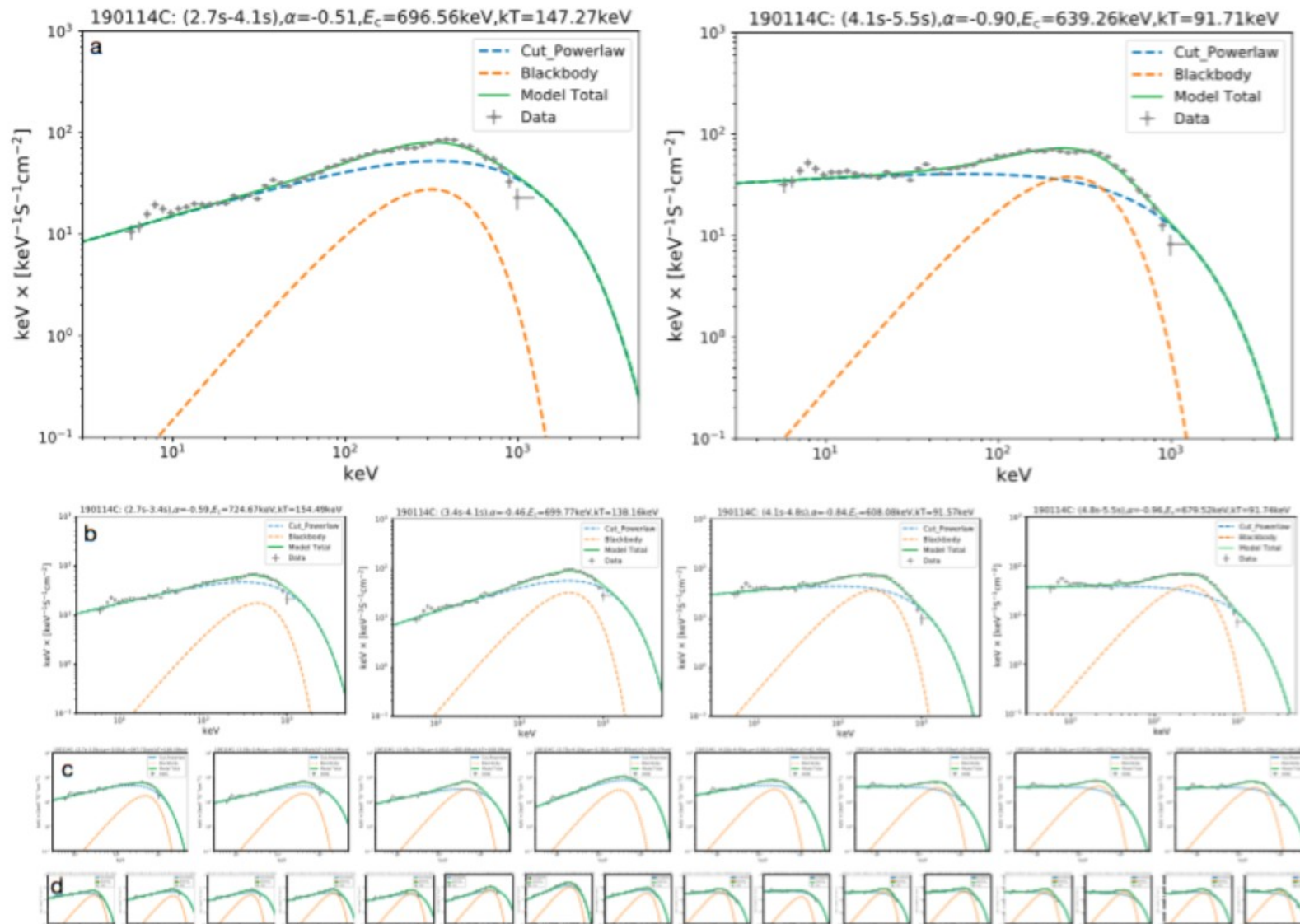
The rotational energy extraction from the Kerr BH: GRB 180720B
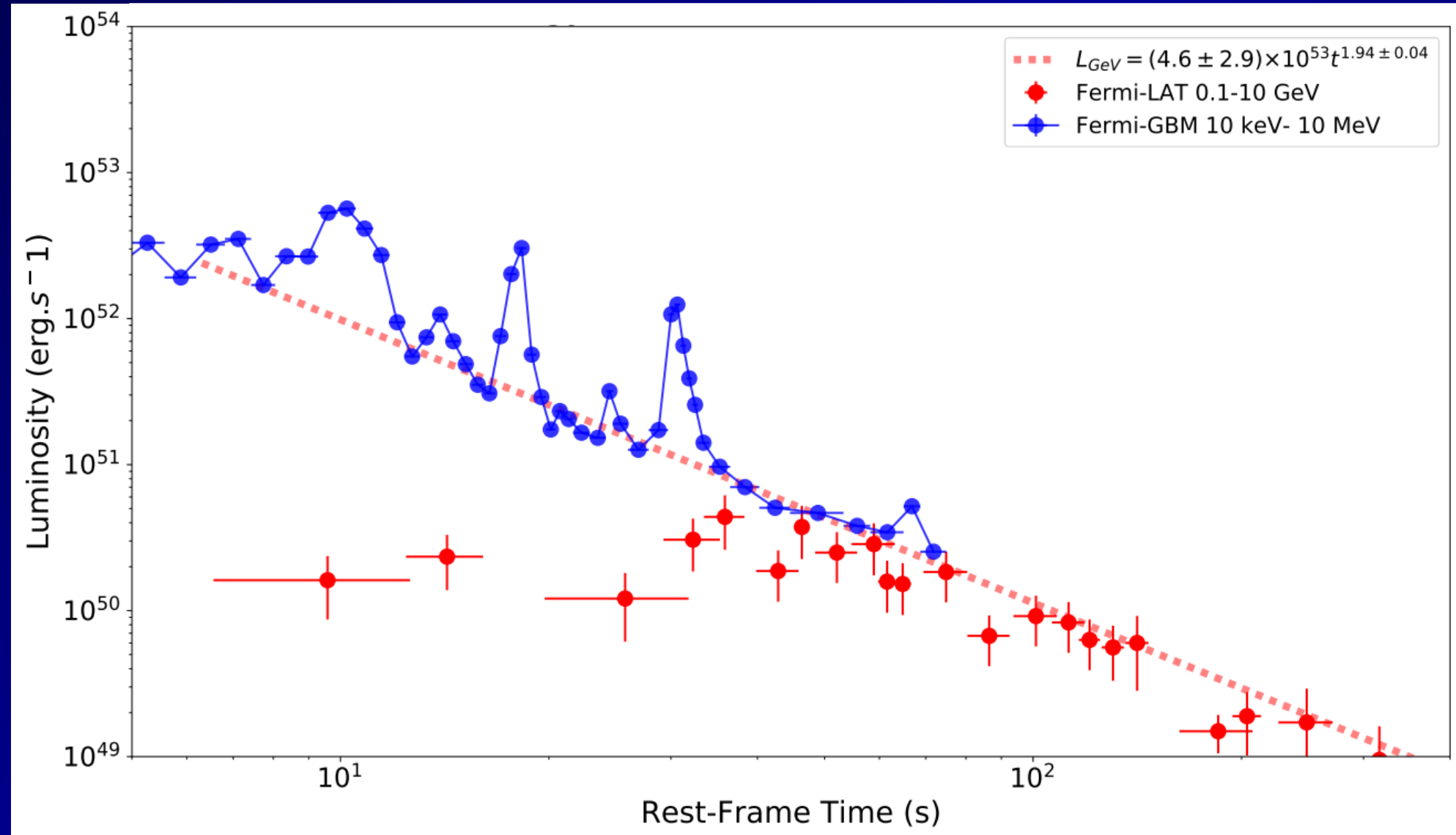
X-ray afterglow from the spinning vNS
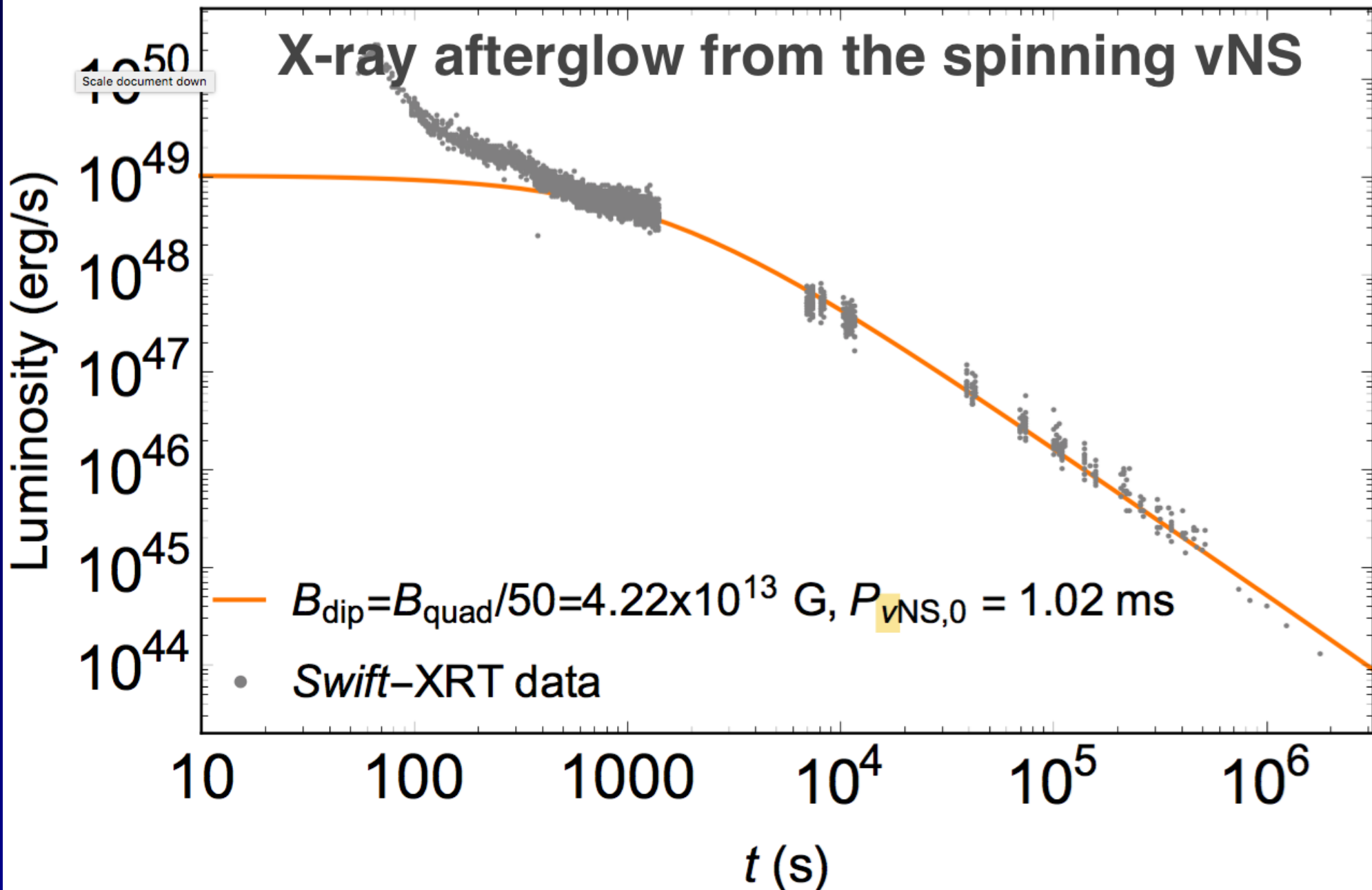
$B_{dip}=B_{quad}/50=4.22 \times 10^{13}$ G, $P_{vNS,0} = 1.02$ ms

Swift−XRT data
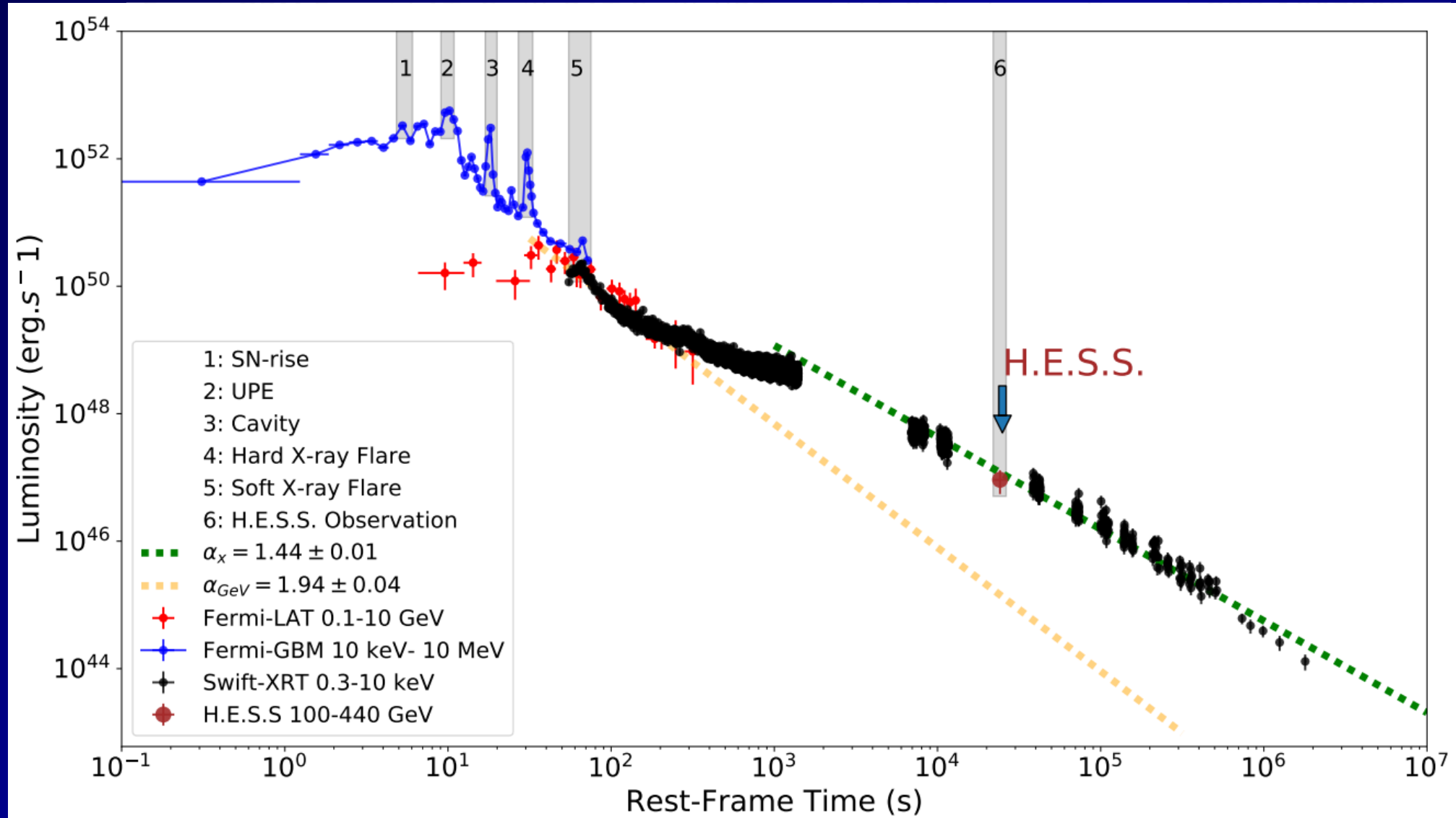
Time-resolved spectral analysis of UPE phase of GRB 180720B

Liang Li et al, today

$t_1 \sim t_2$ (s) Obs	$t_1 \sim t_2$ (s) Rest	S	α	E_c (keV)	kT (keV)	ΔDIC	F_{BB} (10^{-6}) (erg cm^{-2} s^{-1})	F_{tot} (10^{-6}) (erg cm^{-2} s^{-1})	F_{ratio}	E_{tot} (10^{52}) erg
(1)	(2)	(3)	(4)	(5)	(6)	(7)	(8)	(9)	(10)	(11)
15.00~18.00	9.07~10.89	274.60	$-1.06^{+0.01}_{-0.01}$	$1502.5^{+88.6}_{-87.5}$	$39.8^{+1.6}_{-1.6}$	-226.4	$1.99^{+0.43}_{-0.34}$	$45.55^{+3.11}_{-2.70}$	$0.04^{+0.01}_{-0.01}$	$16.0^{+1.1}_{-0.952}$
15.00~16.50	9.07~9.98	190.63	$-1.04^{+0.01}_{-0.01}$	$1750.5^{+112.7}_{-111.1}$	$40.5^{+2.0}_{-2.0}$	-176.6	$2.08^{+0.58}_{-0.46}$	$48.03^{+3.28}_{-3.09}$	$0.04^{+0.01}_{-0.01}$	$8.46^{+0.577}_{-0.543}$
16.50~18.00	9.98~10.89	215.76	$-1.05^{+0.02}_{-0.02}$	$1151.3^{+117.3}_{-119.6}$	$37.1^{+2.8}_{-2.8}$	-78.7	$1.63^{+0.69}_{-0.54}$	$41.83^{+4.61}_{-4.04}$	$0.04^{+0.02}_{-0.01}$	$7.37^{+0.812}_{-0.712}$
15.00~15.75	9.07~9.53	105.93	$-1.07^{+0.03}_{-0.02}$	$1198.0^{+211.1}_{-217.8}$	$31.4^{+3.3}_{-3.3}$	-41.5	$0.94^{+0.70}_{-0.42}$	$23.84^{+4.65}_{-3.86}$	$0.04^{+0.03}_{-0.02}$	$2.1^{+0.41}_{-0.34}$
15.75~16.50	9.53~9.98	168.59	$-0.92^{+0.02}_{-0.02}$	$1028.0^{+74.9}_{-73.9}$	$74.8^{+20.8}_{-25.7}$	-15.4	$0.14^{+0.37}_{-0.13}$	$58.57^{+5.42}_{-4.80}$	$0.0^{+0.01}_{-0.0}$	$5.16^{+0.478}_{-0.423}$
16.50~17.25	9.98~10.44	155.67	$-1.15^{+0.02}_{-0.02}$	$2382.3^{+217.5}_{-221.3}$	$45.3^{+2.7}_{-2.7}$	-125.6	$2.85^{+1.00}_{-0.76}$	$53.96^{+4.55}_{-4.28}$	$0.05^{+0.02}_{-0.01}$	$4.75^{+0.401}_{-0.377}$
17.25~18.00	10.44~10.89	159.05	$-0.93^{+0.02}_{-0.02}$	$684.7^{+49.7}_{-49.2}$	$23.9^{+3.8}_{-4.0}$	-30.8	$0.63^{+0.93}_{-0.37}$	$35.74^{+3.28}_{-3.21}$	$0.02^{+0.03}_{-0.01}$	$3.15^{+0.289}_{-0.283}$
15.00~15.38	9.07~9.30	69.11	$-1.06^{+0.07}_{-0.07}$	$711.2^{+209.5}_{-215.5}$	$28.9^{+5.7}_{-5.6}$	-30.2	$0.78^{+1.14}_{-0.55}$	$14.27^{+6.80}_{-3.54}$	$0.05^{+0.08}_{-0.04}$	$0.628^{+0.299}_{-0.156}$
15.38~15.75	9.30~9.53	83.03	$-1.01^{+0.03}_{-0.03}$	$1319.4^{+210.9}_{-208.7}$	$31.0^{+5.2}_{-5.2}$	-28.9	$0.83^{+1.14}_{-0.48}$	$32.18^{+6.45}_{-5.45}$	$0.03^{+0.04}_{-0.02}$	$1.42^{+0.284}_{-0.24}$
15.75~16.12	9.53~9.75	109.59	$-1.02^{+0.02}_{-0.02}$	$1967.9^{+193.8}_{-194.9}$	$43.6^{+4.0}_{-4.0}$	-72.6	$2.63^{+1.51}_{-0.96}$	$62.61^{+6.83}_{-6.58}$	$0.04^{+0.02}_{-0.02}$	$2.76^{+0.301}_{-0.29}$
16.12~16.50	9.75~9.98	133.10	$-1.01^{+0.02}_{-0.02}$	$1919.4^{+162.1}_{-168.5}$	$47.9^{+3.5}_{-3.5}$	-107.5	$4.31^{+1.60}_{-1.38}$	$82.08^{+8.46}_{-7.17}$	$0.05^{+0.02}_{-0.02}$	$3.61^{+0.372}_{-0.316}$
16.50~16.88	9.98~10.21	133.12	$-1.09^{+0.02}_{-0.02}$	$2574.3^{+264.0}_{-267.2}$	$55.7^{+3.8}_{-3.7}$	-117.9	$5.16^{+2.03}_{-1.44}$	$83.97^{+8.79}_{-7.60}$	$0.06^{+0.02}_{-0.02}$	$3.7^{+0.387}_{-0.335}$
16.88~17.25	10.21~10.44	89.16	$-1.24^{+0.05}_{-0.05}$	$1537.9^{+522.7}_{-558.0}$	$31.9^{+3.8}_{-3.4}$	-27.8	$1.38^{+0.94}_{-0.57}$	$24.25^{+7.37}_{-6.29}$	$0.06^{+0.04}_{-0.03}$	$1.07^{+0.325}_{-0.277}$
17.25~17.62	10.44~10.66	125.76	$-0.86^{+0.03}_{-0.03}$	$696.1^{+59.2}_{-57.7}$	$22.5^{+3.8}_{-3.7}$	-27.3	$0.83^{+1.39}_{-0.48}$	$45.89^{+5.21}_{-4.69}$	$0.02^{+0.03}_{-0.01}$	$2.02^{+0.23}_{-0.206}$
17.62~18.00	10.66~10.89	102.97	$-1.02^{+0.04}_{-0.04}$	$622.4^{+77.4}_{-80.6}$	$25.7^{+8.4}_{-9.5}$	-25.5	$0.39^{+1.32}_{-0.34}$	$25.51^{+4.95}_{-3.40}$	$0.02^{+0.05}_{-0.01}$	$1.12^{+0.218}_{-0.15}$
15.00~15.19	9.07~9.19	51.57	$-1.01^{+0.14}_{-0.15}$	$805.3^{+449.1}_{-380.0}$	$33.0^{+13.1}_{-18.2}$	-288.8	$0.80^{+5.09}_{-0.77}$	$19.23^{+23.49}_{-7.86}$	$0.04^{+0.27}_{-0.04}$	$0.423^{+0.517}_{-0.173}$
15.19~15.38	9.19~9.30	42.03	$-1.19^{+0.09}_{-0.09}$	$1201.3^{+667.6}_{-595.4}$	$27.5^{+4.3}_{-4.2}$	-27.1	$0.97^{+1.06}_{-0.55}$	$12.89^{+8.98}_{-4.04}$	$0.08^{+0.1}_{-0.05}$	$0.284^{+0.198}_{-0.0889}$
15.38~15.56	9.30~9.41	53.84	$-1.00^{+0.04}_{-0.04}$	$1158.5^{+201.4}_{-200.2}$	$23.4^{+8.3}_{-8.3}$	-27.1	$0.29^{+1.66}_{-0.26}$	$27.59^{+7.34}_{-4.93}$	$0.01^{+0.06}_{-0.01}$	$0.608^{+0.162}_{-0.109}$
15.56~15.75	9.41~9.53	63.61	$-1.06^{+0.05}_{-0.05}$	$1839.8^{+434.0}_{-420.6}$	$39.4^{+7.6}_{-7.0}$	-32.2	$1.74^{+2.60}_{-1.11}$	$40.95^{+11.15}_{-9.24}$	$0.04^{+0.06}_{-0.03}$	$0.902^{+0.246}_{-0.203}$
15.75~15.94	9.53~9.64	72.54	$-1.04^{+0.04}_{-0.04}$	$1896.8^{+350.9}_{-351.5}$	$40.8^{+4.7}_{-4.7}$	-30.3	$2.78^{+2.13}_{-1.19}$	$51.44^{+12.23}_{-9.91}$	$0.05^{+0.04}_{-0.03}$	$1.13^{+0.269}_{-0.218}$
15.94~16.12	9.64~9.75	83.99	$-0.99^{+0.03}_{-0.03}$	$1950.2^{+231.8}_{-232.1}$	$47.5^{+7.6}_{-4.7}$	-34.3	$2.34^{+3.12}_{-1.29}$	$74.72^{+11.53}_{-9.35}$	$0.03^{+0.04}_{-0.02}$	$1.65^{+0.254}_{-0.206}$
16.12~16.31	9.75~9.87	85.09	$-0.95^{+0.04}_{-0.03}$	$1379.2^{+207.4}_{-203.8}$	$32.7^{+5.4}_{-5.3}$	-39.2	$1.84^{+2.29}_{-1.02}$	$63.06^{+12.29}_{-10.56}$	$0.03^{+0.04}_{-0.02}$	$1.39^{+0.271}_{-0.233}$
16.31~16.50	9.87~9.98	104.94	$-1.05^{+0.02}_{-0.02}$	$2304.7^{+260.1}_{-261.8}$	$62.1^{+2.8}_{-2.8}$	-85.4	$6.72^{+1.63}_{-1.29}$	$97.87^{+12.08}_{-9.75}$	$0.07^{+0.02}_{-0.01}$	$2.15^{+0.266}_{-0.215}$
16.50~16.69	9.98~10.10	107.18	$-1.04^{+0.03}_{-0.03}$	$2737.1^{+346.9}_{-340.9}$	$58.4^{+5.6}_{-5.6}$	-86.1	$6.57^{+3.89}_{-2.56}$	$119.20^{+16.65}_{-14.38}$	$0.06^{+0.03}_{-0.02}$	$2.62^{+0.367}_{-0.317}$
16.69~16.88	10.10~10.21	82.58	$-1.13^{+0.13}_{-0.08}$	$1910.0^{+709.1}_{-1074.0}$	$58.6^{+8.6}_{-9.2}$	-86.9	$3.67^{+4.06}_{-3.43}$	$53.29^{+28.29}_{-22.24}$	$0.07^{+0.08}_{-0.07}$	$1.17^{+0.623}_{-0.49}$
16.88~17.06	10.21~10.32	64.96	$-1.24^{+0.03}_{-0.03}$	$2412.4^{+580.9}_{-576.0}$	$34.7^{+4.0}_{-4.0}$	-28.1	$1.52^{+1.46}_{-0.72}$	$32.97^{+6.96}_{-5.49}$	$0.05^{+0.05}_{-0.02}$	$0.726^{+0.153}_{-0.121}$
17.06~17.25	10.32~10.44	62.39	$-1.06^{+0.08}_{-0.08}$	$480.3^{+112.6}_{-114.6}$	$21.1^{+8.8}_{-8.9}$	-125.2	$0.39^{+3.01}_{-0.35}$	$15.20^{+8.60}_{-3.47}$	$0.03^{+0.2}_{-0.02}$	$0.335^{+0.189}_{-0.0764}$
17.25~17.44	10.44~10.55	81.92	$-0.89^{+0.05}_{-0.05}$	$720.6^{+93.9}_{-92.3}$	$19.1^{+3.9}_{-3.8}$	-23.5	$0.82^{+1.62}_{-0.55}$	$38.20^{+8.11}_{-5.42}$	$0.02^{+0.04}_{-0.01}$	$0.841^{+0.179}_{-0.119}$
17.44~17.62	10.55~10.66	97.68	$-0.84^{+0.05}_{-0.05}$	$713.4^{+96.8}_{-97.0}$	$32.3^{+11.9}_{-10.7}$	-38.1	$1.05^{+5.66}_{-0.87}$	$55.49^{+13.70}_{-10.34}$	$0.02^{+0.1}_{-0.02}$	$1.22^{+0.302}_{-0.228}$
17.62~17.81	10.66~10.78	82.29	$-0.95^{+0.05}_{-0.05}$	$628.7^{+86.6}_{-86.2}$	$19.5^{+9.9}_{-7.8}$	-66.8	$0.33^{+4.15}_{-0.30}$	$33.47^{+9.11}_{-5.06}$	$0.01^{+0.12}_{-0.01}$	$0.737^{+0.201}_{-0.111}$
17.81~18.00	10.78~10.89	64.36	$-1.08^{+0.06}_{-0.06}$	$565.9^{+123.9}_{-118.5}$	$30.2^{+7.8}_{-10.3}$	-15.3	$0.36^{+1.63}_{-0.33}$	$17.96^{+6.32}_{-3.42}$	$0.02^{+0.09}_{-0.02}$	$0.395^{+0.139}_{-0.0752}$

The morphology of the X-ray afterglows and of the jetted GeV emission in long GRBs

R. Ruffini,[1,2,5,7,13] R. Moradi,[1,2,15]* J. A. Rueda,[1,2,4,8,16] L. Li,[1,2,15] N. Sahakyan,[1,6] Y.-C. Chen,[1,2]
Y. Wang,[1,2,15] Y. Aimuratov,[1,2,9] L. Becerra,[1,2,17] C. L. Bianco,[1,2,16] C. Cherubini,[1,3,11] S. Filippi,[1,3,10]
M. Karlica,[1,2] G. J. Mathews,[1,12] M. Muccino,[15] G. B. Pisani,[1,2] and S. S. Xue[1,2]

[1] ICRANet, Piazza della Repubblica 10, I-65122 Pescara, Italy
[2] ICRA, Dipartimento di Fisica, Università di Roma "La Sapienza", Piazzale Aldo Moro 5, I-00185 Roma, Italy
[3] ICRA, Università Campus Bio-Medico di Roma, Via Alvaro del Portillo 21, I-00128 Rome, Italy
[4] ICRANet-Ferrara, Dipartimento di Fisica e Scienze della Terra, Università degli Studi di Ferrara, Via Saragat 1, I–44122 Ferrara, Italy
[5] ICRANet-Rio, Centro Brasileiro de Pesquisas Físicas, Rua Dr. Xavier Sigaud 150, 22290–180 Rio de Janeiro, Brazil
[6] ICRANet-Armenia, Marshall Baghramian Avenue 24a, Yerevan 0019, Republic of Armenia
[7] Université de Nice Sophia-Antipolis, Grand Château Parc Valrose, Nice, CEDEX 2, France
[8] Dipartimento di Fisica e Science della Terra, Università degli Studi di Ferrara, Via Saragat 1, I-44122 Ferrara, Italy
[9] Fesenkov Astrophysical Institute, Observatory 23, 050020 Almaty, Kazakhstan
[10] Department of Engineering, University Campus Bio-Medico of Rome, Nonlinear Physics and Mathematical Modeling Lab,
Via Alvaro del Portillo 21, 00128 Rome, Italy
[11] Department of Science and Technology for Humans and the Environment and Nonlinear Physics and Mathematical Modeling Lab,
University Campus Bio-Medico of Rome, Via Álvaro del Portillo 21, 00128 Rome, Italy
[12] Center for Astrophysics, Department of Physics, University of Notre Dame, Notre Dame, IN, 46556, USA
[13] Istituto Nazionale di Fisica Nucleare, Laboratori Nazionali di Frascati, I-00044 Frascati, Italy
[14] INAF, Viale del Parco Mellini 84, 00136 Roma, Italy
[15] INAF – Osservatorio Astronomico d'Abruzzo, Via M. Maggini snc, I-64100, Teramo, Italy
[16] INAF, Istituto di Astrofisica e Planetologia Spaziali, Via Fosso del Cavaliere 100, 00133 Rome, Italy
[17] Instituto de Astrofísica, Facultad de Física, Pontificia Universidad Católica de Chile, Av. Vicuña Mackenna 4860, Macul, Santiago, Chile

ABSTRACT

We recall evidence that all long gamma-ray bursts (GRBs) have binary progenitors and give new examples. Binary-driven hypernovae (BdHNe) consist of a carbon-oxygen core (CO_{core}) and a neutron star (NS) companion. For binary periods ~ 5 min, the subclass BdHN I originates from the CO_{core} collapse. BdHN I are characterized by: 1) an energetic supernova (the "SN-rise"); 2) a newborn black hole (BH) originating from the NS collapse by SN matter accretion. The BH produces via the "inner engine" a GeV emission with luminosity $L_{GeV} = A_{GeV} t^{-\alpha_{GeV}}$, observed only in some cases. 3) The new NS (νNS) created from the SN originates the X-ray afterglow with $L_X = A_X t^{-\alpha_X}$, present in all BdHN I. We recall 378 BdHN I and, for four prototypes GRBs 130427A, 160509A, 180720B and 190114C, present: 1) their spectra, luminosities, SN-rise duration; 2) A_X, $\alpha_X = 1.48 \pm 0.32$, and 3) the νNS spin time-evolution. We also infer: a) A_{GeV} and $\alpha_{GeV} = 1.19 \pm 0.04$; b) the BH mass and spin; c) the BdHN I morphology, aided by a time-resolved spectral analysis and three-dimensional simulations. We analyze the presence/absence of GeV emission in 54 sources observed within the Fermi-LAT 75° boresight angle. For 25 sources, we give the integrated and the time-varying GeV emission. The remaining 29 sources have no GeV emission detected, and limit X- and gamma-ray flares previously inferred to be observed along the binary plane. The 25/54 ratio implies the GeV radiation is emitted within a cone of half-opening angle ≈ 60° from the normal to the orbital plane. We estimate the BH masses based upon the *inner engine* originating the GeV emission by extracting the BH rotational energy. We deduce BH initial masses $2.3 < M/M_\odot < 8.9$, spin $0.27 < a/M < 0.87$, and follow their time evolution thereby verifying the validity of the BH mass-energy formula.

Key words: gamma-ray bursts: general — binaries: general — stars: neutron — supernovae: general — black hole physics

1 INTRODUCTION

The year 2021 marks the 50th anniversary of the paper "Introducing the black hole" (Ruffini & Wheeler 1971) and of the black hole (BH) mass-energy formula (Christodoulou 1970; Christodoulou & Ruffini 1971; Hawking 1971; Hawking 1972). Since those days, in
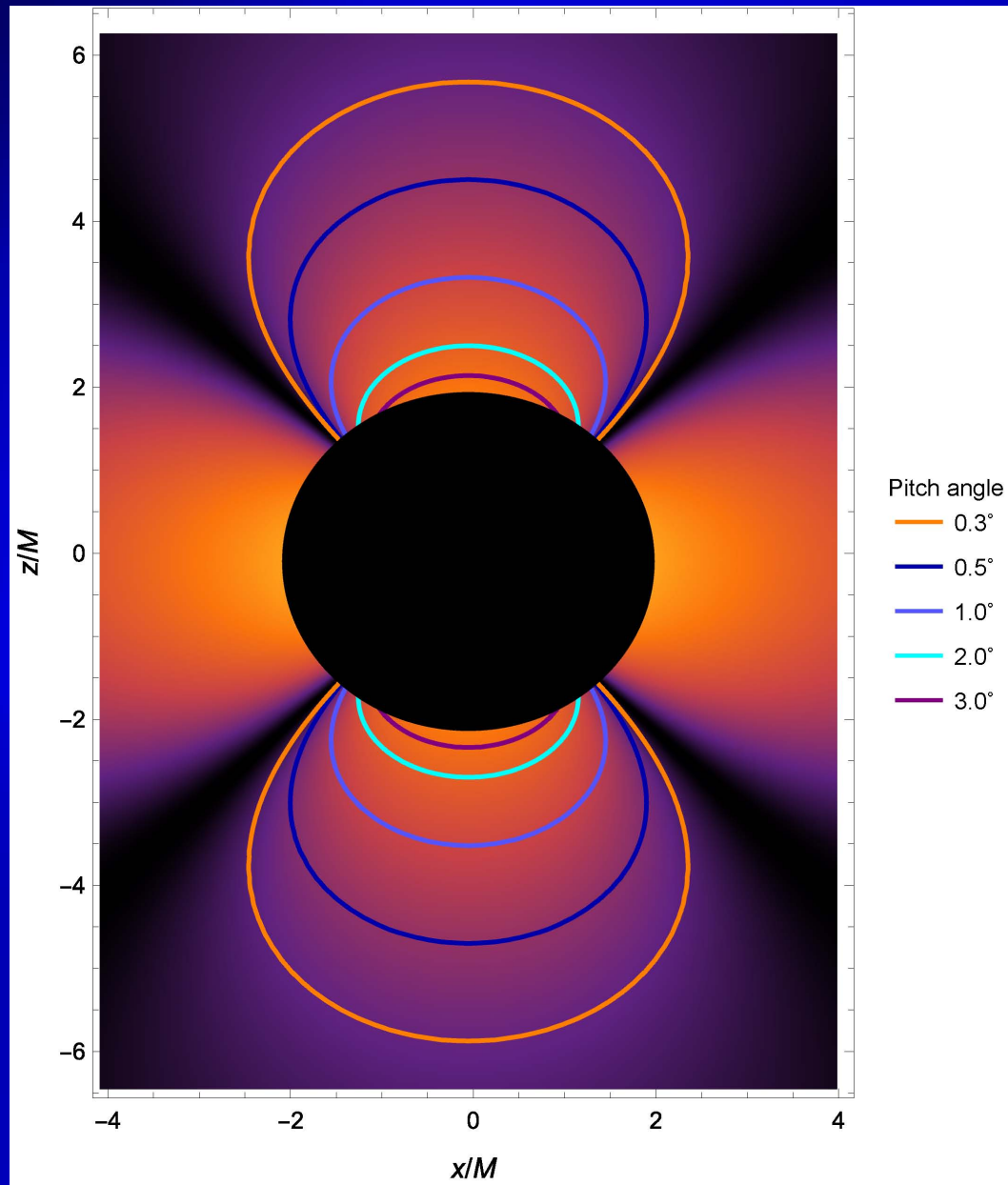
* ruffini@icra.it,　　　　rahim.moradi@inaf.it,　　　　liang.li@icranet.org, jorge.rueda@icra.it, yu.wang@icranet.org
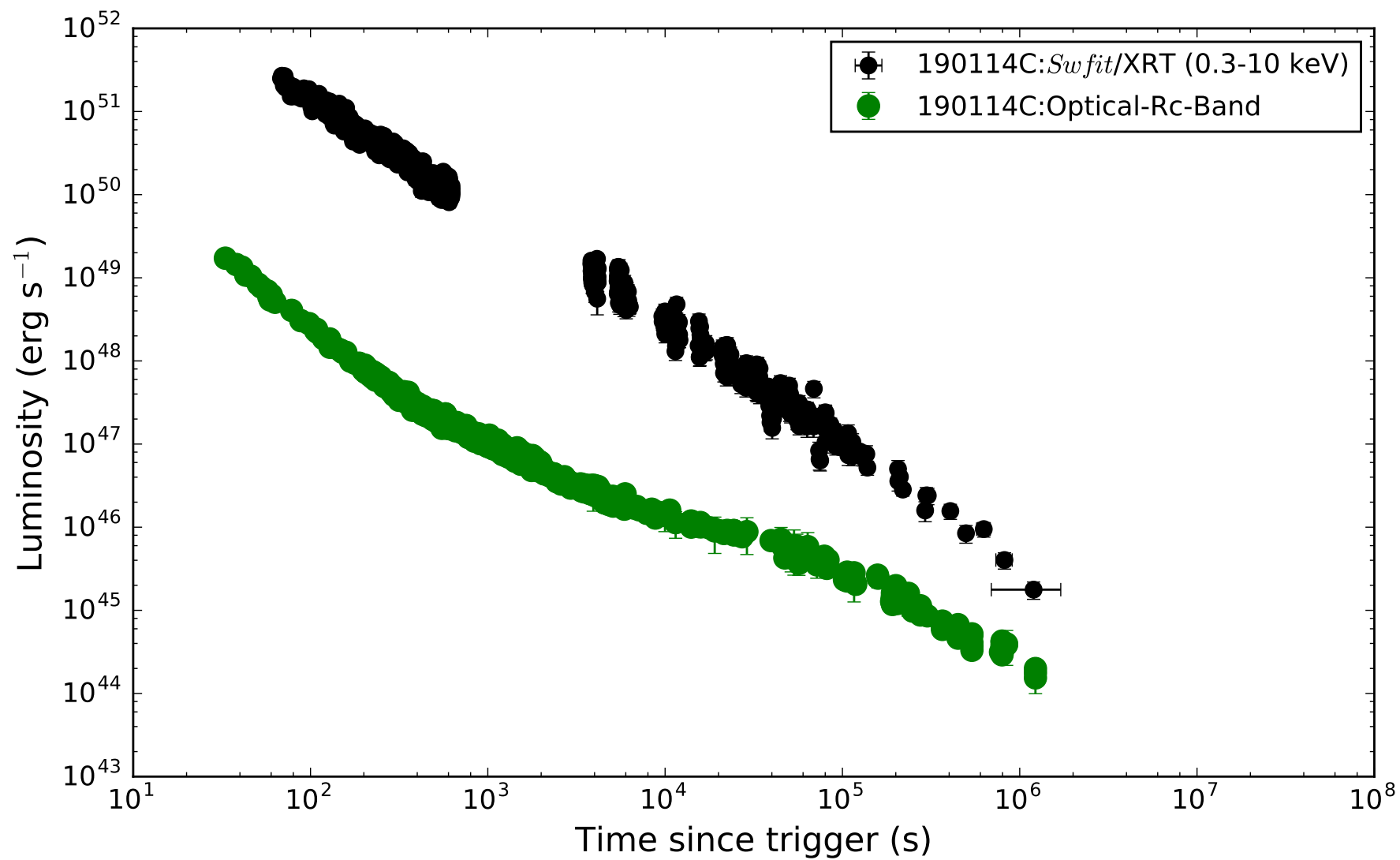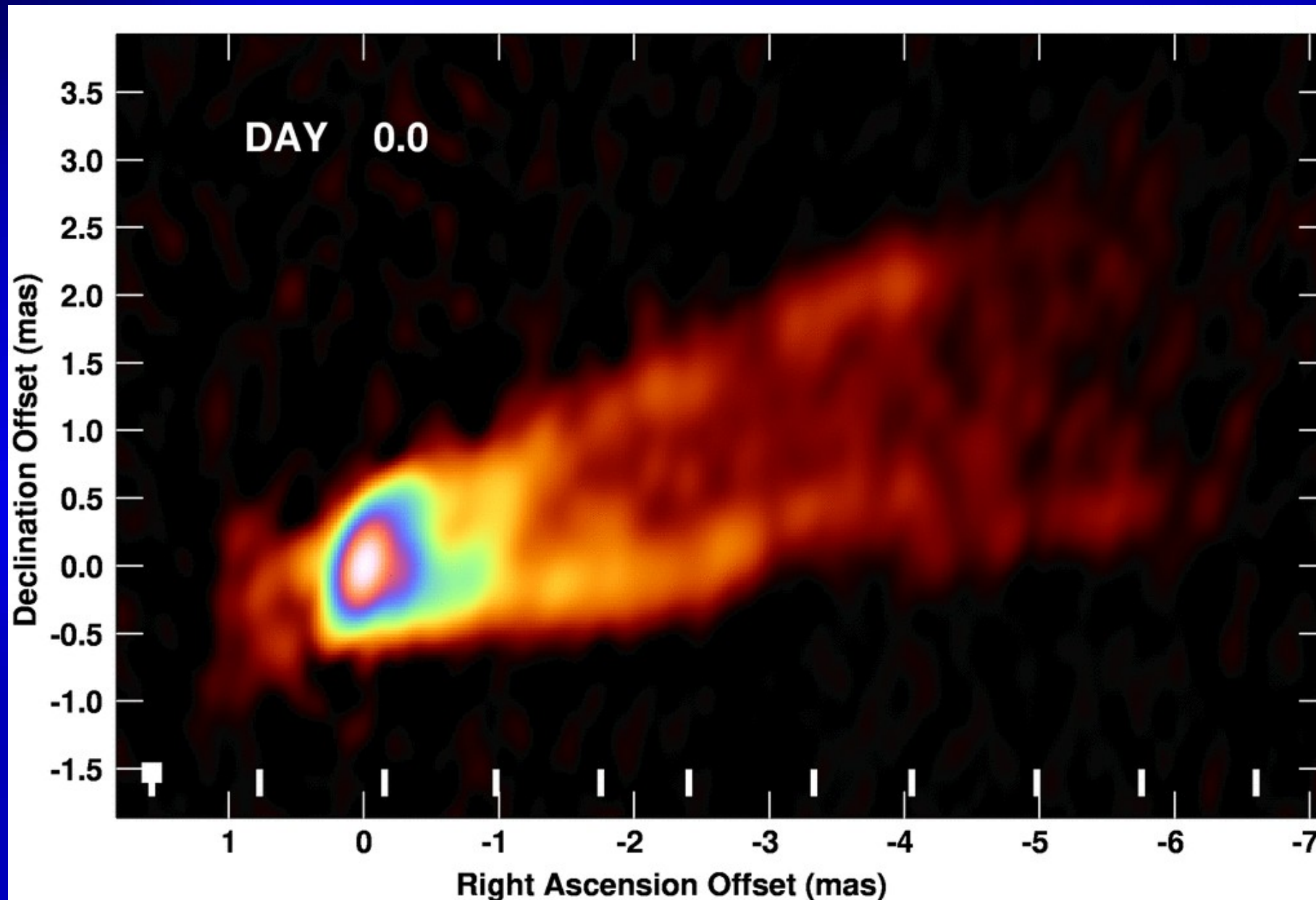
Liang Li, Della Valle, Moradi, Ruffini, Today

The jetted structure of the GeV emission of GRB 190114 C

R. Moradi, J. Rueda, R. Ruffini, Y. Wang, 2021

Can we see the Blackholic quantum?

A general conclusion

We have 380 BdHNI all characterised by a cosmological redshift, an E_{iso} larger than 10+52 erg, and an afterglow. The Afterglow Luminosities have been obtained from the Xray observations of SWIFT. When expressed in the rest frame of the source they fulfill a power law

$$L_X(t) = A_x t^{-1.14\pm0.32}$$

This determine from the BdHNI theory the initial mass and spin of the νNS. Of these 380 BdHNI, in view of their special conical morphology and the boresight angle of the FERMI LAT detector , only 25 BdHN are observed to emit GeV radiation with a luminosity

$$L_n = A_n t^{-1.19\pm0.04}$$

from these observations and the theory of the" Inner engine" we
can infer the BH Mass and Spin for each GeV emitting GRB.

THESEUS

Transient High-Energy Sky and Early Universe Surveyor

THESUS is a space telescope mission proposal by the European Space Agency and is designed to vastly increase the discovery space of the high energy transient phenomena over the entirety of cosmic history. Its primary scientific goals will address the Early Universe ESA Cosmic Vision themes "How did the Universe originate and what is made of?" and will also impact on "The gravitational wave Universe" and "The hot and energetic Universe" themes. This is achieved via a unique payload providing an unprecedented combination of:

1) wide and deep sky monitoring in a broad energy band (0.3 keV - 20 MeV);
2) focusing capabilities in the soft X-ray band providing large grasp and high angular resolution; and
*3) on board near-IR capabilities for immediate transient identification and redshift determination.*

Thanks to...

All the undergraduate, Ph.D. students, post-docs, researchers, faculty and collaborators who participated to this work in the last 40 years.

Among them at ICRANet Seats:

Y. Aimuratov, U. Barres de Almeida, L. Becerra, D. Begue, R. Belvedere, M.G. Bernardini, C.L. Bianco, Cai Yifu (蔡一夫), L. Caito, R. Camargo, P. Chardonnet, Chen Yen-Chen (陈彦蓁), C. Cherubini, F. Cipolletta, A. Corsi, M.G. Dainotti, T. Damour, G. De Barros, M. Della Valle, M. Enderli, Feng Longlong (冯珑珑), S. Filippi, F. Fraschetti, C. Fryer, P. Giommi, R. Guida, L. Izzo, Jing Yipeng (景益鹏), M. Kovacevic, Li Lixin (李 立新), Li Miao (李淼), Liang Li (李亮), G. Mathews, R. Moradi, M. Muccino, Nan Zhang Shuang (张双南), B. Patricelli, A.V. Penacchioni, G.B. Pisani, G. Preparata, L.J. Rangel Lemos, M. Rotondo, J. Rueda, N. Sahakian, J. Salmonson, Shude Mao (毛 书德), Tam Pak-Hin (谭栢轩), G. Vereshchagin, Wang Yu (王瑜), J. Wilson, Xiang Shuoping (向守平), Xue She-Sheng (薛社生), Yau Shing Tung (邱成桐), Yefei Yuan (袁业飞), E. Zaninoni.
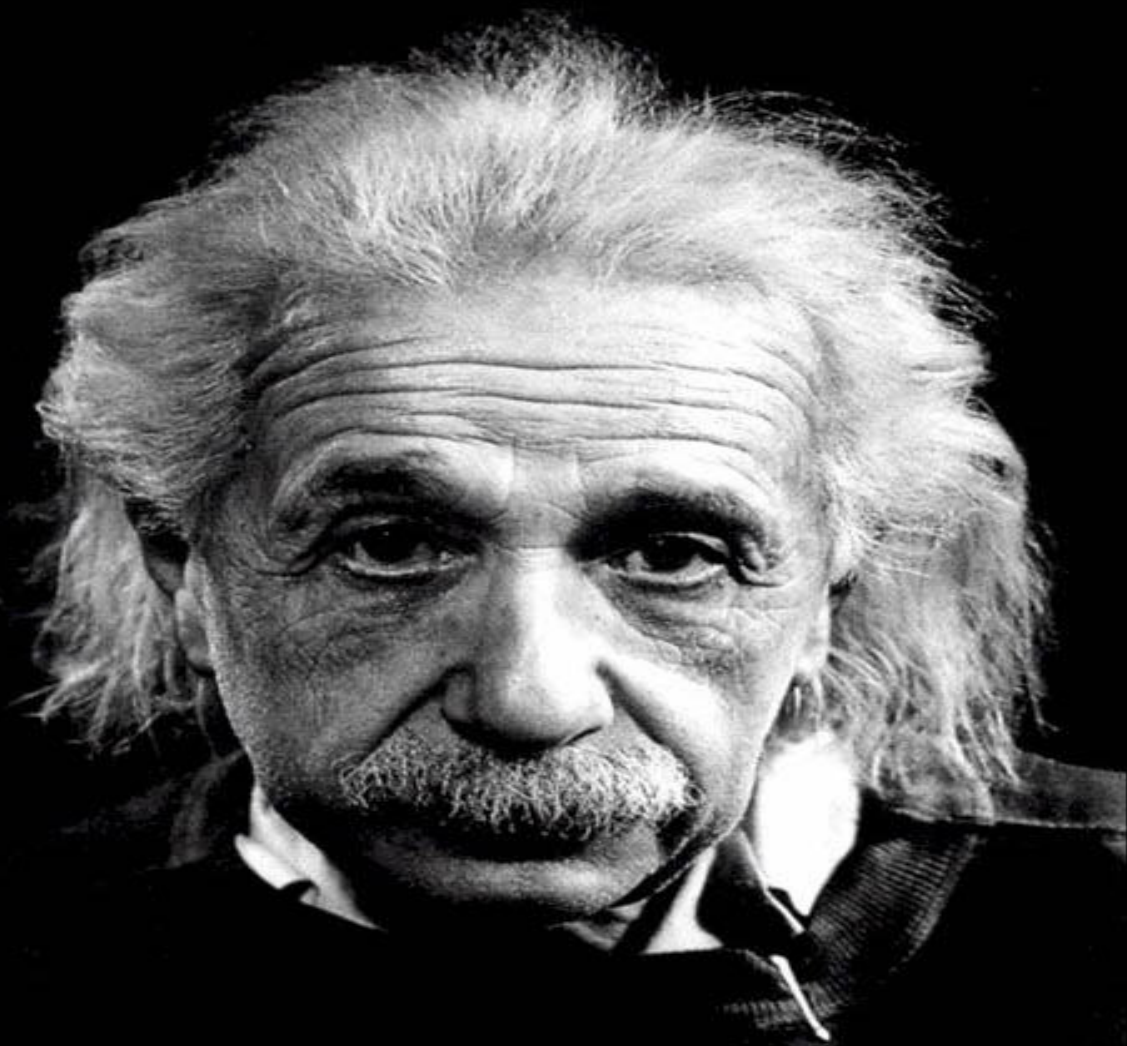
"*The new cosmology will probably turn out to be philosophically even more revolutionary than relativity or the quantum theory*"

P. A. M. Dirac, Scott Lecture